

# Factorization in One-Loop Gauge Theory

Zvi Bern and Gordon Chalmers\*

*Department of Physics  
UCLA  
Los Angeles, CA 90024*

## ABSTRACT

Factorization properties of one-loop gauge theory amplitudes have been used as checks on explicitly computed amplitudes and in the construction of ansätze for higher-point ones. In massless theories, such as QCD at high energies, infrared divergences complicate factorization. Here we prove that factorization in such theories is described by a set of universal functions. In particular, a proof of the universality of one-loop splitting functions as the momenta of two particles become collinear is presented. Factorization in multi-particle channels is also given. The discontinuity functions that appear in the splitting functions may also be used to obtain infrared divergent box integral functions from finite ones.

---

\* Address after September 1, 1995: Institute for Theoretical Physics, SUNY, Stony Brook, NY 11794.

## 1. Introduction

In recent years a variety of one-loop gauge theory amplitudes with five or more external legs, including all virtual corrections to three-jet production at hadron colliders [1,2,3], have been computed. A number of formal developments in computational techniques, including spinor helicity methods [4], string-based methods [5,6], supersymmetry relations [7], recursive techniques [8,9], and unitarity methods [10,11] have allowed the computation of a large variety of new amplitudes.

Factorization properties [12,1,13,10,3] provide strong consistency checks on newly computed amplitudes. Furthermore, they provide a means for obtaining higher-point amplitudes from lower-point ones. To do this one constructs a function that has the correct factorization properties in all channels, which is then an ansatz for the amplitude. An explicit construction of  $n$ -gluon amplitudes with all identical helicities derived from this technique has been given in refs. [13,14] and verified via recursive techniques [9].

The limiting form of one-loop massless gauge theory amplitudes as the momenta of two legs become collinear has been given, although not proven, in terms of splitting functions in previous papers [13,15,10,3]. In particular, a tabulation of the splitting functions in QCD has been given in refs. [10,3] from the collinear limits of calculated five-point amplitudes. Ample evidence of the universality of the splitting functions is provided by the large number of explicitly known one-loop helicity amplitudes in massless gauge theory [5,16,1,2,14,13,9,10,11]. For multi-particle factorization less information is available; except for the recently computed set of one-loop six-point amplitudes in  $N = 4$  supersymmetric gauge theory [11], no examples have been constructed with non-trivial factorization properties. (Mahlon [9] has also constructed a set of helicity amplitudes containing multi-particle poles, but with simple factorization properties due to a lack of infrared singularities.) Other properties at loop level which are known are for the unpolarized differential cross-sections, and give the well known Altarelli-Parisi splitting functions [17]. The Altarelli-Parisi splitting functions are for cross-sections which include both real emission and virtual diagrams; the splitting functions that we discuss in this paper are for the virtual (i.e. loop) diagrams alone.

In this paper we provide a general proof of the universal behavior of massless amplitudes, independent of the number of legs, when factorized on a collinear or multi-particle pole. Amplitudes which lack infrared divergences factorize straightforwardly as one would expect. For amplitudes with infrared singularities the situation is more subtle: massless gauge theory amplitudes generally do *not* factorize in any simple sense since there are contributions which cannot be interpreted directly in terms of lower-point amplitudes. Nevertheless, we will prove here that the non-factorization may be described in terms of a small set of *factorization functions*, given in this paper, whose coefficients are fixed by the known infrared divergences. We also give a practical procedure for calculating the splitting functions of any one-loop amplitude from two- and three-point diagrams.

In previous papers [13,15] proofs of the universality of the (two-particle) one-loop splitting functions for the case of  $n$  external gluons with a virtual scalar loop were outlined. (This was sufficient for the particular helicity amplitudes considered in these papers, because of supersymmetry identities [7] which relate the contributions of virtual gluons and fermions to those of scalars.) The

proof was based on an analysis of Feynman diagrams in the limit that the momenta of two external legs become collinear. This type of proof also works for a fermion loop [18], but a generalization to the case of virtual gluons and multi-particle factorization is non-trivial due to complications in quantifying non-factorizing contributions.

One expects, however, that the universality of the splitting functions should follow from general field theory considerations and not from the details of particular diagrams. Our proof will make this explicit and is valid for any particle content and external states. The key behind the proof is that we can link all non-factorizing contributions to infrared divergences present in the one-loop amplitudes. We will show that only a small number of functions may enter and that their coefficients are fixed by their infrared divergences. Since the divergences have a known form [19,20,21], all functions entering into factorization are fixed and universal; this is the main result of this paper.

A spin-off from our analysis is that the same functions that contribute to the loop splitting functions may also be used to efficiently obtain all infrared divergent box integrals by taking limits of known infrared finite massive box integrals [22]. To illustrate this, we reproduce the box integrals necessary for calculating amplitudes in massless gauge theory given in ref. [23].

First, in Section 2 we review some properties of gauge theory amplitudes that we will find useful in our subsequent discussion. In Section 3 we present our results for the one-loop splitting functions; an explicit sample calculation is presented for obtaining the splitting functions from three-point diagrams. In section 4 we present analogous results for multi-particle factorization and a non-trivial example. The actual proof of these results are presented in Section 5 and the appendices. In section 6 we show that the same functions which appear in the non-factorizing contributions are useful for obtaining infrared divergent box integral functions from infrared finite ones. We also provide a variety of appendices on integrals and their properties which are useful in the proof.

## 2. Review of Previous Results

We now briefly review some previous results and conventions that we will use in this paper: the color ordering of non-abelian scattering amplitudes, the spinor helicity method, tree-level two-particle collinear limits and the structure of infrared and ultraviolet singularities. We review (and slightly modify) the integral reduction method for calculating any one-loop integral in terms of box, triangle and bubble functions in appendix I.

### 2.1 Color-Ordered Amplitudes

Tree-level  $SU(N_c)$  gauge theory amplitudes can be written in terms of independent color-ordered partial amplitudes multiplied by an associated color trace [24]. This is extensively discussed in the review article of Mangano and Parke [25], whose normalizations and conventions we follow. (In particular, we normalize fundamental representation color matrices as  $\text{Tr}[T^a T^b] = \delta^{ab}$ .) One of the key features of the partial amplitudes is that the external legs have a fixed ordering.

At one-loop, although the analogous decomposition [26] is a bit more complicated, gauge theory amplitudes may be conveniently written in terms of gauge-invariant ‘primitive’ amplitudes

[3] which also have fixed ordering of external legs. The  $n$ -gluon primitive amplitudes correspond to the leading-color partial amplitudes,  $A_{n;1}^{\text{loop}}$ . Furthermore, the complete amplitude may be expressed in terms of appropriate permutation sums over primitive amplitudes multiplied by ordered color factors. Therefore, all results obtained in this paper for primitive amplitudes may be converted to results for full amplitudes. For amplitudes with only external gluons, or two quarks and the rest gluons, explicit expressions giving the full amplitudes in terms of these primitive amplitudes may be found in refs. [10,3]. For this paper, the main property needed is that a decomposition of one-loop  $SU(N_c)$  gauge theory amplitudes exists in terms of a set of color decomposed amplitudes where the ordering of external legs is fixed; this is convenient, although not necessary for our discussion.

## 2.2 Spinor Helicity

In explicit calculations it is usually convenient to use a spinor helicity basis [4], where all quantities are rewritten in terms of Weyl spinors  $|k^\pm\rangle$ . In the formulation of Xu, Zhang and Chang the polarization vectors are expressed as

$$\varepsilon_\mu^{(+)}(k; q) = \frac{\langle q^- | \gamma_\mu | k^- \rangle}{\sqrt{2} \langle q k \rangle}, \quad \varepsilon_\mu^{(-)}(k, q) = \frac{\langle q^+ | \gamma_\mu | k^+ \rangle}{\sqrt{2} [k q]}, \quad (2.1)$$

where  $q$  is an arbitrary null ‘reference momentum’ which drops out of the final gauge-invariant amplitudes. The reader is referred to the article of Xu, Zhang and Chang for further details. For the purposes of this presentation we note that

$$\langle k_i^- | k_j^+ \rangle \equiv \langle ij \rangle = \sqrt{2k_i \cdot k_j} \exp(i\phi), \quad \langle k_i^+ | k_j^- \rangle \equiv [ij] = -\sqrt{2k_i \cdot k_j} \exp(-i\phi), \quad (2.2)$$

where  $\phi$  is a phase. These spinor products vanish in the limit  $k_i \cdot k_j \rightarrow 0$ , are anti-symmetric and satisfy

$$\langle ij \rangle [j i] = 2k_i \cdot k_j. \quad (2.3)$$

## 2.3 Tree-Level Two-particle Collinear Factorization

Consider first an  $n$ -point tree-level partial amplitude  $A_n^{\text{tree}}(1, 2, \dots, n)$  with a fixed ordering of external legs and an arbitrary helicity configuration  $(\lambda_1, \lambda_2, \dots, \lambda_n)$ , where each  $\lambda_i = \pm$ . As the momenta of two *neighboring* legs  $a$  and  $b$  become collinear the leading behavior of the amplitudes is given by [27,12]

$$A_n^{\text{tree}} \xrightarrow{a||b} \sum_{\lambda=\pm} \text{Split}_{-\lambda}^{\text{tree}}(a^{\lambda_a}, b^{\lambda_b}) A_{n-1}^{\text{tree}}(\dots K^\lambda \dots), \quad (2.4)$$

where the non-vanishing splitting functions (or amplitudes) diverge as  $1/\sqrt{s_{ab}}$  in the collinear limit  $s_{ab} = (k_a + k_b)^2 \rightarrow 0$ . In this equation and all subsequent ones we extract all coupling constants from the color-ordered amplitudes. The collinear limit is defined by  $k_a = zK$  and  $k_b = (1-z)K$ , where the null vector  $K$  is the sum of the collinear momenta;  $\lambda$  is the helicity of the intermediate state with momentum  $K$ . The tree splitting functions  $\text{Split}_{-\lambda}^{\text{tree}}(a^{\lambda_a}, b^{\lambda_b})$  may be found in ref. [25].

The  $g \rightarrow gg$  splitting functions are

$$\begin{aligned} \text{Split}_{-}^{\text{tree}}(a^{-}, b^{-}) &= 0, & \text{Split}_{-}^{\text{tree}}(a^{+}, b^{+}) &= \frac{1}{\sqrt{z(1-z)}\langle ab \rangle}, \\ \text{Split}_{-}^{\text{tree}}(a^{+}, b^{-}) &= -\frac{z^2}{\sqrt{z(1-z)}[ab]}, & \text{Split}_{-}^{\text{tree}}(a^{-}, b^{+}) &= -\frac{(1-z)^2}{\sqrt{z(1-z)}[ab]}, \end{aligned} \quad (2.5)$$

which explicitly exhibit the  $1/\sqrt{s_{ab}}$  pole. All remaining  $g \rightarrow gg$  splitting functions may be obtained by parity.

## 2.4 Infrared and Ultraviolet Singularities in One-Loop Amplitudes

In massless gauge theory one encounters three types of singularities when evaluating virtual corrections with fixed particle number. Besides the usual ultraviolet singularities one encounters both soft and collinear infrared ones. (By ‘soft’ we refer to the  $\epsilon^{-2}$  terms in dimensionally regulated amplitudes.) These types of singularities must cancel in final physical cross-sections containing both real and virtual corrections, but are present in the individual parts. The singularities in an  $n$ -point massless QCD amplitude with a fixed ordering of legs are of the form [19,20,21]

$$A_n^{\text{loop}} \Big|_{\text{singular}} = c_{\Gamma} A_n^{\text{tree}} \left[ -\frac{1}{\epsilon^2} \sum_{j=1}^n \mathcal{S}_j^{[n]} \left( \frac{\mu^2}{-s_{j,j+1}} \right)^{\epsilon} + \mathcal{C}^{[n]} \frac{1}{\epsilon} \right], \quad (2.6)$$

where

$$c_{\Gamma} = \frac{(4\pi)^{\epsilon}}{16\pi^2} \frac{\Gamma(1+\epsilon)\Gamma^2(1-\epsilon)}{\Gamma(1-2\epsilon)}, \quad (2.7)$$

with  $\epsilon = (4-D)/2$  the dimensional regularization parameter and  $\mu$  the renormalization scale. The parameters  $\mathcal{S}_j^{[n]}$  are the coefficients of the soft singularities and  $\mathcal{C}^{[n]}$  is the sum of the coefficients of collinear and ultraviolet divergences, which depend on the particle content of the amplitude. Although we will write the soft singularities in the form appearing in eq. (2.6), the functional form of the amplitudes are taken, as usual, to be expanded in  $\epsilon$ . This expansion is implied in eq. (2.6) and in all subsequent expressions.

The main property that we will make use of is that in massless QCD the coefficients  $\mathcal{S}_j^{[n]}$  and  $\mathcal{C}^{[n]}$  are known. For primitive amplitudes which have been stripped of all color factors and have a fixed ordering of legs, these coefficients are particularly simple. For such amplitudes,  $\mathcal{S}_j^{[n]}$  is 0 or 1 depending on the particle type of the internal loop line connecting legs  $j$  and  $j+1$  in the ‘parent diagram’, which is the one where all external legs are directly attached to the loop by three-vertices. If the propagator between legs  $j$  and  $j+1$  is a gluon then  $\mathcal{S}_j^{[n]} = 1$ , while if it is a fermion or scalar then  $\mathcal{S}_j^{[n]} = 0$ . (Explicit examples are found in ref. [3].)

The collinear infrared singularities for  $n$ -point amplitudes are

$$\mathcal{C}_{\text{IR}}^{[n]} = -\sum_{a=1}^n \gamma(a), \quad (2.8)$$

where the sum is over all  $n$  legs and depends on whether leg  $a$  is a gluon  $g$  or a fermion  $q$ ,

$$\begin{aligned}\gamma(g) &= \frac{11}{6} - \frac{1}{3} \frac{n_f}{N_c} - \frac{1}{6} \frac{n_s}{N_c}, \\ \gamma(q) &= \frac{3}{4} \left(1 - \frac{1}{N_c^2}\right),\end{aligned}\tag{2.9}$$

where  $n_f$  is the number of fermions,  $n_s$  the number of scalars (which is zero in QCD) and  $N_c$  the number of colors. Our conventions follow the ones in refs. [1,10,3]; in particular we have extracted an overall factor of  $N_c$  from leading color amplitudes so that contributions from fundamental representation loops carry a factor of  $1/N_c$ . The normalization for each complex scalar is non-standard and represents a total of four states in the  $(N_c + \bar{N}_c)$  representation (instead of the usual two; the rationale for this choice is to maintain supersymmetry identities with the four states of fundamental representation Dirac fermions). There are also ultraviolet singularities

$$\mathcal{C}_{\text{UV}}^{[n]} = (n-2) \left( \frac{11}{6} - \frac{1}{3} \frac{n_f}{N_c} - \frac{1}{6} \frac{n_s}{N_c} \right).\tag{2.10}$$

The coefficient  $\mathcal{C}^{[n]}$  appearing in eq. (2.6) is the sum

$$\mathcal{C}^{[n]} = \mathcal{C}_{\text{UV}}^{[n]} + \mathcal{C}_{\text{IR}}^{[n]},\tag{2.11}$$

of the infrared and ultraviolet contributions in eqs. (2.8) and (2.10).

### 3. Collinear Limits

#### 3.1 General Results

In this section we present our results for the factorization of one-loop amplitudes as the momenta of two color-adjacent external legs become collinear; in subsequent sections we present the proof. The behavior of one-loop amplitudes in the collinear limit found from explicit calculations of amplitudes with five or more legs, is [1,10,3]

$$A_n^{\text{loop}} \xrightarrow{a\parallel b} \sum_{\lambda=\pm} \left\{ \text{Split}_{-\lambda}^{\text{tree}}(a^{\lambda_a}, b^{\lambda_b}) A_{n-1}^{\text{loop}}(\dots K^\lambda \dots) + \text{Split}_{-\lambda}^{\text{loop}}(a^{\lambda_a}, b^{\lambda_b}) A_{n-1}^{\text{tree}}(\dots K^\lambda \dots) \right\},\tag{3.1}$$

where the  $A_n^{\text{loop}}$  and  $A_n^{\text{tree}}$  are color-decomposed one-loop and tree amplitudes with a fixed ordering of legs and  $a$  and  $b$  are consecutive in the ordering. This is a natural generalization of the tree-level factorization and is exactly what one would expect in massive theories with no infrared divergences, since in this case individual diagrams respect the factorization depicted in fig. 1, where legs  $i$  and  $i+1$  correspond to  $a$  and  $b$ .

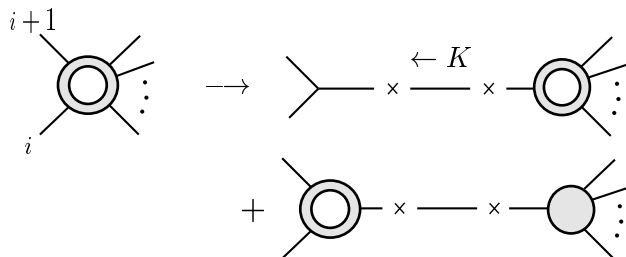


Figure 1. The ‘naive’ factorization of one-loop amplitudes in the limit as two external momenta become collinear, where  $K = k_i + k_{i+1}$ . The shaded disc represents the sum over tree diagrams and the annulus the sum over one-loop diagrams.

For infrared divergent theories the situation is much more subtle since individual diagrams may not have a smooth behavior as the intermediate momentum becomes massless. We shall, however, prove that the splitting functions  $\text{Split}_{-\lambda}^{\text{loop}}$  are independent of the number of external legs  $n$ , and that they may be obtained by calculating three-point diagrams followed by adding in a particular set of functions fixed by the singularities in  $\epsilon$  through eq. (2.6).

The following analysis is performed on bare amplitudes (before renormalization). For massless amplitudes it is slightly more convenient to leave all quantities as bare, but at any point in the discussion one may convert to renormalized quantities by performing the appropriate ultraviolet subtraction in all quantities; this will be done for the final splitting functions. We will also use the dimensional reduction [28] or equivalently the four-dimensional helicity (FDH) regularization schemes [5]. These schemes are convenient since they do not introduce any  $\epsilon$ -dependence coming from the contraction of tensors which count the number of states circulating in the loop. It is straightforward to convert the splitting functions to conventional [29] or 't Hooft-Veltman schemes [30]; through  $\mathcal{O}(\epsilon^0)$  the splitting functions shift by constants multiplied by tree splitting functions, as given in refs. [10,3]. A discussion of scheme conversions has been given in ref. [16].

In general, infrared divergent amplitudes will not factorize naively. As a simple example of non-factorization, consider an infrared singularity of the form

$$-c_{\Gamma} \frac{1}{\epsilon^2} (-s_{23})^{-\epsilon} A_n^{\text{tree}} = -c_{\Gamma} \left[ \frac{1}{\epsilon^2} - \frac{1}{\epsilon} \ln(-s_{23}) + \dots \right] A_n^{\text{tree}}, \quad (3.2)$$

in the collinear limit  $k_1 = zK$  and  $k_2 = (1-z)K$ . This singularity contains the logarithmic term

$$\frac{1}{\epsilon} \ln(-s_{23}) \rightarrow \frac{1}{\epsilon} \ln(-(1-z)s_{K3}), \quad (3.3)$$

with  $k_i^2 = 0$ , which introduces a  $\ln(1-z)/\epsilon$  not belonging with either the ‘naively factorized’ diagrams on the left- or right-hand-side of the tree-pole in fig. 1 (for  $i = 1$ ). It therefore cannot be interpreted as a factorizing contribution.

Our results for the limits of amplitudes as legs  $i$  and  $i+1$  become collinear ( $k_i \rightarrow zK$  and  $k_{i+1} \rightarrow (1-z)K$ ) are as follows. As the two legs become collinear, loop integrals may not have smooth limits and develop infrared divergences. The possible discontinuities, which describe the off-shell to on-shell transition, are described by a set of universal ‘discontinuity functions’. Two discontinuity functions which play an explicit role in computing the loop splitting functions are

$$\begin{aligned} b(s_{i,i+1}) &= \frac{1}{\epsilon(1-2\epsilon)} \left( \frac{\mu^2}{-s_{i,i+1}} \right)^{\epsilon}, \\ d_1(s_{i,i+1}) &= \frac{1}{\epsilon^2} \left( \frac{\mu^2}{-s_{i,i+1}} \right)^{\epsilon}. \end{aligned} \quad (3.4)$$

(There are additional discontinuity functions to be discussed in section 5, but they are not needed for our discussion of the factorizing diagrams.)

Now consider the computation of loop splitting functions which are composed of factorizing and non-factorizing pieces,

$$\text{Split}^{\text{loop}} = \text{Split}^{\text{fact}} + \text{Split}^{\text{non-fact}}. \quad (3.5)$$

The first step in obtaining the factorizing contributions is to compute the diagrams depicted in fig. 2. Observe that diagrams with bubbles on external lines are not included. This is due to the dimensional regularization prescription that massless on-shell bubble diagrams vanish [31], which is interpreted as a complete cancellation of infrared and ultraviolet divergences. (Below we also describe the diagrams necessary for calculating the splitting functions in a massive theory.) The diagrams in fig. 2 yield the general form

$$\mathcal{D} = B_2 \frac{1}{\epsilon^2} \left( \frac{\mu^2}{-s_{i,i+1}} \right)^\epsilon + B_1 \frac{1}{\epsilon} + B_0, \quad (3.6)$$

where  $B_1$  and  $B_2$  are rational functions depending on the particle content and on the type of external legs. Depending on the type of off-shell leg, represented by the dotted line in fig. 2,  $\mathcal{D}$  may have uncontracted spinor or vector indices.

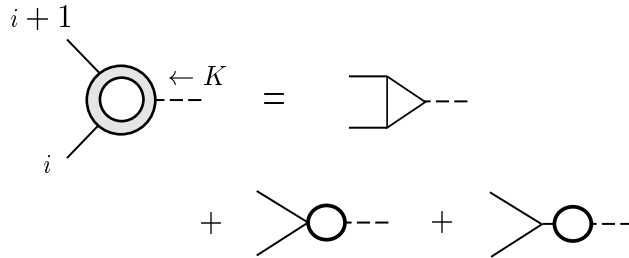


Figure 2. The diagrams in a massless theory (ignoring tadpoles) that need to be calculated to obtain the factorizing contribution to the loop splitting function. The dotted line represents the off-shell leg on which the collinear factorization is performed.

It is convenient to collect all singular terms, including those in eq. (3.6), into the non-factorizing category. We achieve this by subtracting all singularities in  $\epsilon$  from eq. (3.6) using the discontinuity functions (3.4), and then adding them back into the non-factorizing set discussed below. This collects all non-smooth behavior into the non-factorizing contributions. (In general, the coefficients of the singularities,  $B_1$  and  $B_2$ , depend on gauge choices and the processes under consideration.) Subtracting out the divergences from the factorizing diagrams yields

$$\mathcal{D}' = B_2 \left[ \frac{1}{\epsilon^2} \left( \frac{\mu^2}{-s_{i,i+1}} \right)^\epsilon - d_1(s_{i,i+1}) \right] + B_1 \left[ \frac{1}{\epsilon} - b(s_{i,i+1}) \right] + B_0, \quad (3.7)$$

which we label as the ‘factorizing’ contribution to the splitting functions. By construction this is completely free of singularities in  $\epsilon$ . The result  $\mathcal{D}'$  may then be contracted against the  $(n-1)$ -point tree diagrams, as in the last diagram in fig. 1, and converted to an expression in terms of spinor helicity. The conversion is performed by inserting a complete set of helicity states on the intermediate factorized leg and then taking the collinear limit; this yields

$$\sum_{\lambda=\pm} \text{Split}_{-\lambda}^{\text{fact}}(i, i+1) A_{n-1}^{\text{tree}}(\dots K^\lambda \dots). \quad (3.8)$$

In this way we obtain the factorizing contribution to the loop splitting functions. In the next sub-section we present an explicit example.



The second type of contribution is the ‘non-factorizing’ one, which comes from non-smooth behavior in any of the diagrams. This includes the non-smooth contributions which were subtracted from the diagrams in fig. 2 and any other diagrams which generate kinematic poles from the loop integrals. These contributions are proportional to discontinuity functions (3.4) and a limited set of integral functions containing poles in  $s_{i,i+1}$  to be discussed in section 5.

We find that the non-factorizing contributions to the loop splitting functions are proportional to the tree-level splitting functions, so we have

$$\text{Split}_{-\lambda}^{\text{non-fact}}(a^{\lambda_a}, b^{\lambda_b}) = c_{\Gamma} \times \text{Split}_{-\lambda}^{\text{tree}}(a^{\lambda_a}, b^{\lambda_b}) \times r_S(a, b), \quad (3.9)$$

where  $r_S$  contains no spinor products or helicity dependence, and  $a$  and  $b$  are legs  $i$  and  $i + 1$ . The contributions to  $r_S$  are given in Table 1 in terms of the singularities of the amplitudes (2.6). The proportionality of  $\text{Split}^{\text{non-fact}}$  to  $\text{Split}^{\text{tree}}$  follows from the appearance of singularities in all non-factorizing contributions and from the proportionality of the singularities in loop amplitudes to tree amplitudes.

In Table 1 the coefficients for the singularities  $\mathcal{S}_{i-1}^{[n]}$ ,  $\mathcal{S}_i^{[n]}$ ,  $\mathcal{S}_{i+1}^{[n]}$ , and  $\mathcal{C}^{[n]}$  are for the  $n$ -point amplitude, and the coefficient  $\mathcal{C}^{[n-1]}$  is for the  $(n-1)$ -point loop amplitude described by the second set of diagrams on the right-hand-side of fig. 1. The additive contribution to  $r_S$  is given by the coefficient in the first column multiplied by the corresponding terms in the third column. Note that  $r_S$  depends only on the particle types of legs  $i$ ,  $i + 1$  (and the fused leg) through the dependence on  $\mathcal{S}_j^{[n]}$  and  $\mathcal{C}^{[n]} - \mathcal{C}^{[n-1]}$ .

Coefficient	Singularity	Non-Factorizing Contribution to $r_S$
$\mathcal{S}_{i-1}^{[n]}$	$-\frac{1}{\epsilon^2} \left( \frac{\mu^2}{-s_{i-1,i}} \right)^\epsilon$	$\frac{1}{\epsilon^2} \left( \frac{\mu^2}{-s_{i,i+1}} \right)^\epsilon - \frac{1}{\epsilon^2} \left( \frac{\mu^2}{-zs_{i,i+1}} \right)^\epsilon - \text{Li}_2(1-z)$
$\mathcal{S}_{i+1}^{[n]}$	$-\frac{1}{\epsilon^2} \left( \frac{\mu^2}{-s_{i+1,i+2}} \right)^\epsilon$	$\frac{1}{\epsilon^2} \left( \frac{\mu^2}{-s_{i,i+1}} \right)^\epsilon - \frac{1}{\epsilon^2} \left( \frac{\mu^2}{-(1-z)s_{i,i+1}} \right)^\epsilon - \text{Li}_2(z)$
$\mathcal{S}_i^{[n]}$	$-\frac{1}{\epsilon^2} \left( \frac{\mu^2}{-s_{i,i+1}} \right)^\epsilon$	$-\frac{1}{\epsilon^2} \left( \frac{\mu^2}{-s_{i,i+1}} \right)^\epsilon$
$\mathcal{C}^{[n]} - \mathcal{C}^{[n-1]}$	$\frac{1}{\epsilon}$	$\frac{1}{\epsilon(1-2\epsilon)} \left( \frac{\mu^2}{-s_{i,i+1}} \right)^\epsilon$

**Table 1:** The ‘non-factorizing’ contributions to the loop factorization functions in the  $s_{i,i+1}$  channel. The coefficients in the first column are the coefficients of the contributions to  $r_S$  given in the third column.

The first two entries appearing in the third column are the collinear limits of discontinuity functions summed with specific box functions

$$\begin{aligned} d_1(s_{i,i+1}) + \mu^{2\epsilon} F_{n:i+2}^{1m} \Big|_{k_i \| k_{i+1}}, \\ d_1(s_{i,i+1}) + \mu^{2\epsilon} F_{n:i+3}^{1m} \Big|_{k_i \| k_{i+1}}, \end{aligned} \quad (3.10)$$

where  $F_{n:i+2}^{1m}$  and  $F_{n:i+3}^{1m}$  are the single-external-mass (or off-shell) box functions given through  $\mathcal{O}(\epsilon^0)$  in eqs. (IV.14e) and (IV.10e). (The form in eq. (3.10) is valid to any order in  $\epsilon$ .)

The terms of higher order in  $\epsilon$  can become important when performing phase-space integrals for  $n + 1$  parton contributions to  $n$ -jet final states at next-to-next-to-leading-order (NNLO) when using, for example, the formalism of ref. [20]. The splitting functions may be used to compute analytically the phase-space integrals in the collinear regions; in these regions the phase space integrals contain powers of  $\epsilon^{-1}$  which can cancel against higher order terms in the splitting functions to leave finite results. The higher-order in  $\epsilon$  terms in the splitting functions may be obtained (within the dimensional reduction [28] or FDH [5] schemes) by simply keeping as many orders as desired from both the diagrams in eq. (3.7), and from Table 1, using the form in eq. (3.10) for the first two entries. The other functions appearing in the table are given in a form valid to all orders in  $\epsilon$ . In performing the phase space integral it is convenient not to convert to a helicity basis, but to leave all expressions in terms of the formal polarization vectors. (If one were to convert to a helicity form one would have to account for the fact that the momentum over which one performs the phase space integral is actually in  $4 - 2\epsilon$  dimensions and not in four dimensions; this type of subtlety has, however, already been addressed by Mahlon [9] in the context of recursion relations for amplitudes.)

In summary, the total contribution to the loop splitting function (3.5) is given by the sum of the factorizing and non-factorizing contributions. The factorizing contributions (3.8) are independent of the number of external legs since they always come from the same three-point diagrams depicted in fig. 2. The non-factorizing contributions (3.9) are also universal because their coefficients are fixed by the singular terms (2.6). Thus, for any number of external legs the loop splitting functions appearing in eq. (3.1) depend only on the ‘local’ properties within the diagrams: the helicity and particle type of the two collinear legs and the virtual matter content. For the color-ordered primitive amplitudes of ref. [3] the splitting functions also depend on the routing of the fermion through the diagrams.

### 3.2 Collinear Limit Example

As an example, consider a one-loop  $n$ -gluon partial amplitude in a theory with  $n_f$  massless fermions,  $n_s$  massless complex scalars, and  $N_c$  colors in the limit that legs 1 and 2 become collinear:  $k_1 = zK$  and  $k_2 = (1 - z)K$ . First we compute the factorizing contributions by evaluating the two- and three-point loop diagrams of the type in fig. 2 (for  $i = 1$ ); the ones with fermion loops are depicted in fig. 3. The gluon and scalar loop diagrams are similar except that one must include diagrams with four-point contact vertices. In performing the calculation, the intermediate leg (the dashed line) with momentum  $(-k_1 - k_2)$  should be left off-shell in the initial part of the calculation. These diagrams are conveniently evaluated [32] using color-ordered Feynman background field gauge [33] for the loop and Gervais-Neveu gauge [34] for the tree parts of the diagrams. Through all orders

in  $\epsilon$  we have

$$\mathcal{D}_{\text{Background}}^\mu = \frac{i}{\sqrt{2}} \frac{\tau_\Gamma}{3} \left( 1 + \frac{n_s}{N_c} - \frac{n_f}{N_c} \right) \left[ \varepsilon_1 \cdot \varepsilon_2 - \frac{\varepsilon_1 \cdot k_2 \varepsilon_2 \cdot k_1}{k_1 \cdot k_2} \right] (k_1 - k_2)^\mu, \quad (3.11)$$

where

$$\tau_\Gamma \equiv \frac{6}{(4\pi)^{2-\epsilon}} \frac{\Gamma(1+\epsilon)\Gamma^2(1-\epsilon)}{\Gamma(4-2\epsilon)} \left( \frac{\mu^2}{-s_{12}} \right)^\epsilon = \frac{1}{16\pi^2} + \mathcal{O}(\epsilon). \quad (3.12)$$

In the computation we have used the dimensional reduction scheme, while in the conventional [29] or 't Hooft-Veltman [30] schemes there would be an extra overall factor of  $(1-\epsilon)$  in the gluon loop contributions, which has no effect through  $\mathcal{O}(\epsilon^0)$ . The fermions and scalars are taken to be in the fundamental representation. (For the adjoint representation the  $n_s$  and  $n_f$  terms would not have a factor of  $1/N_c$ .) A background field Ward identity between the two and three-point function cancels the divergences between the separate diagrams leaving the finite result in eq. (3.11).

One may of course use other gauges, although in general these yield more complicated expressions. For example, with color-ordered Feynman gauge the gluon loop diagrams are

$$\begin{aligned} \mathcal{D}_{\text{Feynman}}^\mu = & \frac{i}{\sqrt{2}} \left\{ c_\Gamma d_1(s_{12}) \left[ -\frac{3}{4} \varepsilon_1 \cdot \varepsilon_2 (k_1 - k_2)^\mu + \varepsilon_1^\mu \varepsilon_2 \cdot k_1 - \varepsilon_2^\mu \varepsilon_1 \cdot k_2 \right] \right. \\ & + \frac{1}{2} c_\Gamma b(s_{12}) \left[ -\varepsilon_1 \cdot \varepsilon_2 (k_1 - k_2)^\mu + \frac{1}{4} \varepsilon_1 \cdot \varepsilon_2 (k_1 + k_2)^\mu + \varepsilon_2 \cdot k_1 \varepsilon_1^\mu - \varepsilon_1 \cdot k_2 \varepsilon_2^\mu \right] \\ & \left. + \frac{\tau_\Gamma}{3} \left[ \varepsilon_1 \cdot \varepsilon_2 - \frac{\varepsilon_1 \cdot k_2 \varepsilon_2 \cdot k_1}{k_1 \cdot k_2} \right] \left( (k_1 - k_2)^\mu + \frac{1}{8} (3 - 2\epsilon) (k_1 + k_2)^\mu \right) \right\}, \end{aligned} \quad (3.13)$$

which has been written in a form to expose the discontinuity functions (3.4) contained within the diagrams. The result for this gauge (3.13) looks rather different than the one for background field gauge (3.11) and is a reflection of the gauge dependence of the diagrams due to the off-shell intermediate leg.

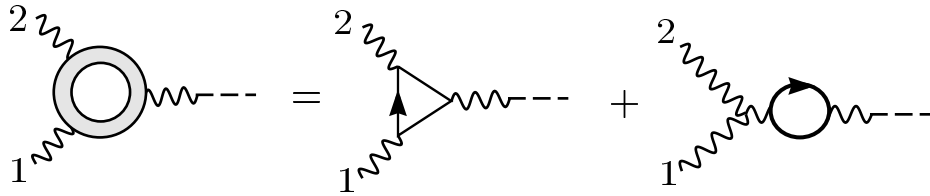


Figure 3. The diagrams for the factorizing massless fermion loop contributions to the  $g \rightarrow gg$  loop splitting functions.

As discussed above, the first step in obtaining the contributions to the loop splitting function after having calculated the factorizing diagrams in fig. 2 (or fig. 3 for fermions) is to push all singularities in  $\epsilon$  into the non-factorizing category using the discontinuity functions (3.4). After moving the singularities from the Feynman gauge result (3.13) into the non-factorizing contributions, it

agrees with the background field gauge result (3.11), up to terms proportional to  $(k_1 + k_2)^\mu$ . Since the free index  $\mu$  contracts against a tree-level conserved current, these terms are irrelevant. Thus, in either gauge, we obtain the ‘factorizing’ contribution as

$$A_n^{\text{fact}} \xrightarrow{1\|2} \left(1 + \frac{n_s}{N_c} - \frac{n_f}{N_c}\right) \frac{\tau_\Gamma}{6} \left[ \varepsilon_1 \cdot \varepsilon_2 - \frac{\varepsilon_1 \cdot k_2 \varepsilon_2 \cdot k_1}{k_1 \cdot k_2} \right] \frac{(k_1 - k_2)^\mu}{\sqrt{2} k_1 \cdot k_2} \eta_{\mu\nu} A_{n-1}^{\text{tree}}(K, 3, \dots, n)^\nu, \quad (3.14)$$

where

$$A_{n-1}^{\text{tree}}(K, 3, \dots, n)^\nu = \frac{\partial}{\partial \varepsilon_\nu(K)} A_{n-1}^{\text{tree}}(K, 3, \dots, n). \quad (3.15)$$

and  $\eta_{\mu\nu}$  is the Minkowski metric. Although we obtain the same result in either gauge, the natural choice for the calculation is background field gauge, since one directly obtains the physical part from eq. (3.11). (The form in eq. (3.14) is valid to higher order in  $\epsilon$  and thus would be the appropriate expression to use for NNLO phase-space integrals.)

The expression (3.14) may be converted to spinor helicity notation by inserting a complete set of helicity states on the intermediate leg [8] using an off-shell generalization of the helicity formalism. For on-shell momentum  $K$  from eq. (2.1) we have

$$\varepsilon_\mu^+(-K, q) \varepsilon_\nu^-(K, q) \equiv \frac{\langle q^- | \gamma_\mu \not{K} \gamma_\nu | q^- \rangle}{2 \langle q^- | \not{K} | q^- \rangle}. \quad (3.16)$$

The right-hand-side of this equation is well defined for off-shell  $K$ , so we may take it as the definition for a product of off-shell polarization vectors; we need only define the product of polarizations since this is the only combination that appears when inserting a complete set of helicity states. It is not difficult to verify with eq. (3.16) the identity

$$\eta_{\mu\nu} = -\varepsilon_\mu^+(-K, q) \varepsilon_\nu^-(K, q) - \varepsilon_\mu^-(-K, q) \varepsilon_\nu^+(K, q) + \frac{K_\mu q_\nu + q_\mu K_\nu}{K \cdot q}, \quad (3.17)$$

which then allows us to replace the  $\eta_{\mu\nu}$  with off-shell polarization vectors plus a piece which will vanish by current conservation. For  $K = k_1 + k_2$  we have

$$(k_2 - k_1) \cdot \varepsilon^+(-K, q) \varepsilon_\nu^-(K, q) = \frac{\langle q k_2^- | [k_2 k_1] \langle k_1^- | \gamma_\nu | q^- \rangle - \langle q k_1^- | [k_1 k_2] \langle k_2^- | \gamma_\nu | q^- \rangle}{2 \langle q^- | \not{K} | q^- \rangle}. \quad (3.18)$$

We parametrize the collinear limit by  $k_1 \rightarrow zK$  and  $k_2 \rightarrow (1-z)K$  with  $K^2 \rightarrow 0$ , to obtain

$$(k_2 - k_1) \cdot \varepsilon^+(-K, q) \varepsilon_\nu^-(K, q) \rightarrow -\sqrt{2z(1-z)} [k_1 k_2] \varepsilon_\nu^-(K, q), \quad (3.19)$$

where the polarization vector on the right-hand side is on-shell. Thus after inserting a complete set of helicity states using eq. (3.17) (through  $\mathcal{O}(\epsilon^0)$ ) we obtain from eq. (3.14)

$$A_n^{\text{fact}} \xrightarrow{1\|2} \left(1 + \frac{n_s}{N_c} - \frac{n_f}{N_c}\right) \sum_{\lambda=\pm} \text{Split}_{-\lambda}^{\text{fact}}(1, 2) A_{n-1}^{\text{tree}}(K^\lambda, 3, \dots, n), \quad (3.20)$$

where

$$\begin{aligned}
\text{Split}_{\pm}^{\text{fact}}(1^+, 2^-) &= \text{Split}_{\pm}^{\text{fact}}(1^-, 2^+) = 0, \\
\text{Split}_{+}^{\text{fact}}(1^+, 2^+) &= -\frac{1}{48\pi^2} \sqrt{z(1-z)} \frac{[12]}{\langle 12 \rangle^2}, \\
\text{Split}_{-}^{\text{fact}}(1^+, 2^+) &= \frac{1}{48\pi^2} \sqrt{z(1-z)} \frac{1}{\langle 12 \rangle},
\end{aligned} \tag{3.21}$$

are the factorizing contributions to the loop splitting functions.

To obtain the non-factorizing contribution to the splitting function we note that for  $n$  external gluons  $\mathcal{S}_i^{[n]} = 1$  for all  $i$  and  $\mathcal{C}^{[n]} = \mathcal{C}^{[n-1]}$ , so that from eq. (2.6) the singular terms in  $\epsilon$  are

$$A_n^{\text{loop}} \Big|_{\text{singular}} = -c_{\Gamma} A_n^{\text{tree}} \left[ \frac{1}{\epsilon^2} \sum_{j=1}^n \left( \frac{\mu^2}{-s_{j,j+1}} \right)^{\epsilon} + \frac{2}{\epsilon} \left( \frac{11}{6} - \frac{1}{3} \frac{n_f}{N_c} - \frac{1}{6} \frac{n_s}{N_c} \right) \right]. \tag{3.22}$$

From Table 1, the non-factorizing contribution to  $r_S$  for this example is the sum of the first three entries in the last column, given by

$$r_S(1, 2) = \frac{1}{\epsilon^2} \left( \frac{\mu^2}{-s_{12}} \right)^{\epsilon} - \frac{1}{\epsilon^2} \left( \frac{\mu^2}{-zs_{12}} \right)^{\epsilon} - \frac{1}{\epsilon^2} \left( \frac{\mu^2}{z(1-z)s_{12}} \right)^{\epsilon} - \text{Li}_2(1-z) - \text{Li}_2(z) + \mathcal{O}(\epsilon). \tag{3.23}$$

After simplifying  $r_S$  using the dilogarithm identity

$$\text{Li}_2(1-z) + \text{Li}_2(z) = -\ln(z) \ln(1-z) + \frac{\pi^2}{6}, \tag{3.24}$$

we obtain from eq. (3.9) the non-factorizing contributions to the  $g \rightarrow gg$  splitting functions,

$$\text{Split}_{-\lambda}^{\text{non-fact}}(1, 2) = c_{\Gamma} \text{Split}_{-\lambda}^{\text{tree}}(1, 2) \left[ -\frac{1}{\epsilon^2} \left( \frac{\mu^2}{z(1-z)(-s_{12})} \right)^{\epsilon} + 2 \ln(z) \ln(1-z) - \frac{\pi^2}{6} \right]. \tag{3.25}$$

Combining the results (3.20) and (3.25) yields the total contribution

$$\text{Split}^{\text{loop}}(1, 2) = \left( 1 + \frac{n_s}{N_c} - \frac{n_f}{N_c} \right) \text{Split}^{\text{fact}}(1, 2) + \text{Split}^{\text{non-fact}}(1, 2), \tag{3.26}$$

in agreement with the results in ref. [10] obtained from taking the explicit collinear limits of five-gluon amplitudes [1].

Finally by performing the ultra-violet subtraction using (2.10) we obtain the corresponding splitting function for renormalized amplitudes as

$$\begin{aligned}
\text{Split}_{\text{ren}}^{\text{loop}}(1, 2) &= \left( 1 + \frac{n_s}{N_c} - \frac{n_f}{N_c} \right) \text{Split}^{\text{fact}}(1, 2) + \text{Split}^{\text{non-fact}}(1, 2) \\
&\quad - c_{\Gamma} \frac{1}{\epsilon} \left( \frac{11}{6} - \frac{1}{3} \frac{n_f}{N_c} - \frac{1}{6} \frac{n_s}{N_c} \right) \text{Split}^{\text{tree}}(1, 2),
\end{aligned} \tag{3.27}$$

where all remaining powers of  $\epsilon^{-1}$  are infrared singularities.

The loop splitting functions for amplitudes with external fermions and gluons may similarly be obtained; these have already been extracted from four- and five-parton calculations and tabulated in refs. [10,3].

### 3.3 Collinear Factorization with Massive Fermions and Scalars

For amplitudes with no infrared singularities the splitting functions are entirely determined by the naively factorizing contributions. Consider, for example, the collinear limit of gluon amplitudes in a theory with massive fermion or scalar loops. Since the mass cuts off any singular behavior as legs go on-shell, all loop integrals are smooth in the collinear limit and the amplitude naively factorizes; the collinear poles only come from external gluon propagators. Thus massive fermion contributions to the splitting functions may be directly determined by calculating only the diagrams in fig. 4. (For a scalar loop there are additional diagrams containing the four-point interaction.)

Following the usual renormalization procedure, half of each bubble on the external line is associated with external wavefunction renormalization. Note that the set of diagrams that contribute to the massive loops is different from that of massless loops (given in fig. 3). The difference between the two sets is due to the dimensional regularization prescription that massless bubbles on external legs vanish; in fig. 3 the two diagrams with bubbles on external lines vanish and are therefore not included. For the massive case in fig. 4 half of the bubble on the ‘internal’ line on which the factorization is being performed belongs with the  $(n - 1)$ -point amplitude and not with the loop splitting function.

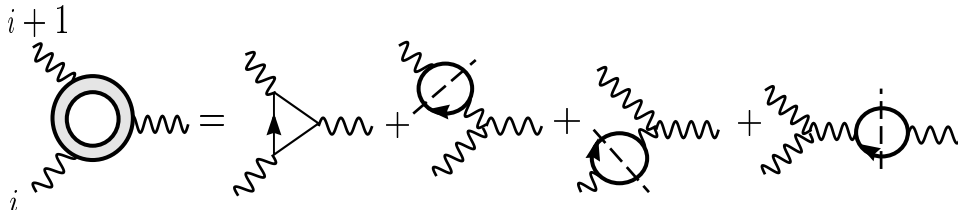


Figure 4. The diagrams representing contributions of massive fermions to the  $g \rightarrow gg$  loop splitting function; the wavy lines represent gluons, and the dashed lines represent the fact that only half of each bubble is included.

The calculation of the diagrams in fig. 4 is straightforward and gives the entire contribution to the loop splitting functions. This gives the contribution of massive fermion and scalar loops to the  $g \rightarrow gg$  splitting functions as\*

$$\text{Split}_{-\lambda}^{\text{loop}}(a, b) = -\frac{1}{3} \frac{1}{(4\pi)^{2-\epsilon}} \Gamma(\epsilon) \left[ \frac{n_f}{N_c} \left( \frac{\mu^2}{m_f^2} \right)^\epsilon + \frac{1}{2} \frac{n_s}{N_c} \left( \frac{\mu^2}{m_s^2} \right)^\epsilon \right] \text{Split}_{-\lambda}^{\text{tree}}(a, b), \quad (3.28)$$

where  $n_f$  and  $n_s$  are the number of fermions and scalars and  $m_f$  and  $m_s$  the corresponding masses.

The proportionality of these contributions to the tree splitting functions may be understood from the structure of the effective action (for  $k_1 \cdot k_2 \ll m^2$ ). The contribution to the effective Lagrangian from a massive fermion or scalar is

$$\mathcal{L}_{\text{eff}} = -\frac{Z_A}{4} F_{\alpha\beta}^a F^{a\alpha\beta} + \mathcal{O}\left(\frac{1}{m^2}\right), \quad (3.29)$$

---

\* As in refs. [1,3], each scalar here contains four states (to match the four states of Dirac fermions) so that  $n_s$  must be divided by two for comparisons to conventional normalizations of scalars.

where  $Z_A$  is the wavefunction renormalization. The higher order terms are suppressed in the collinear limit because they contain  $1/m^2$  instead of  $1/k_1 \cdot k_2$ , leaving only a renormalization of the tree splitting functions. In the massless case this argument breaks down and there is no reason to expect the loop splitting functions to be proportional to the tree ones.

Subtracting off ultra-violet singularities (2.10) from eq. (3.28) gives the splitting functions from massive fermions or scalars for renormalized gluon amplitudes as

$$\text{Split}_{-\lambda}^{\text{renorm}}(a, b) = -\frac{1}{3} \frac{1}{(4\pi)^2} \left[ \frac{n_f}{N_c} \ln\left(\frac{\mu^2}{m_f^2}\right) + \frac{1}{2} \frac{n_s}{N_c} \ln\left(\frac{\mu^2}{m_s^2}\right) \right] \text{Split}_{-\lambda}^{\text{tree}}(a, b) + \mathcal{O}(\epsilon). \quad (3.30)$$

The gluon loop contributions in this theory may be obtained from eq. (3.27) by taking the number of massless scalar and fermions to vanish,  $n_f = n_s = 0$ .

## 4. Multi-particle Factorization

Consider now multi-particle factorization which we will show has analogous behavior to the two-particle collinear limits. As in the latter case, this non-smooth behavior may be linked to the infrared singularities appearing in massless amplitudes.

### 4.1 General Considerations

We will prove that the factorization properties for  $(k_i + k_{i+1} + \dots + k_{i+r-1})^2 = t_i^{[r]} \equiv K^2 \rightarrow 0$  (with  $r > 2$ ) are described by the universal formula,

$$A_n^{\text{loop}} \xrightarrow{K^2 \rightarrow 0} \sum_{\lambda=\pm} \left[ A_{r+1}^{\text{loop}}(k_i, \dots, k_{i+r-1}, K^\lambda) \frac{1}{K^2} A_{n-r+1}^{\text{tree}}(K^{-\lambda}, k_{i+r}, \dots, k_{i-1}) \right. \\ \left. + A_{r+1}^{\text{tree}}(k_i, \dots, k_{i+r-1}, K^\lambda) \frac{1}{K^2} A_{n-r+1}^{\text{loop}}(K^{-\lambda}, k_{i+r}, \dots, k_{i-1}) \right. \\ \left. + A_{r+1}^{\text{tree}}(k_i, \dots, k_{i+r-1}, K^\lambda) \frac{1}{K^2} A_{n-r+1}^{\text{tree}}(K^{-\lambda}, k_{i+r}, \dots, k_{i-1}) c_\Gamma \mathcal{F}_n(K^2; k_1, \dots, k_n) \right], \quad (4.1)$$

where the one-loop *factorization function*  $\mathcal{F}_n$  is independent of helicities. This formula is similar to the one for an amplitude which factorizes naively, as depicted in fig. 5, except that  $\mathcal{F}_n$  may contain kinematic invariants with momenta from both sides of the pole in  $K^2$ ; for example  $\ln(-t_{i-1}^{[2]}) = \ln(-s_{i-1,i})$  is one such logarithm. (In fig. 5 we have made the bubble on the intermediate leg explicit; in fig. 1, for collinear limits, the bubble diagram was implicitly included in the last diagram on the right-hand-side, as depicted in fig. 2.) As for the splitting functions the factorization function is composed of factorizing and non-factorizing components,

$$\mathcal{F}_n = \mathcal{F}_n^{\text{fact}} + \mathcal{F}_n^{\text{non-fact}}. \quad (4.2)$$

For convenience we have extracted an overall factor of  $c_\Gamma$  from the factorization function.

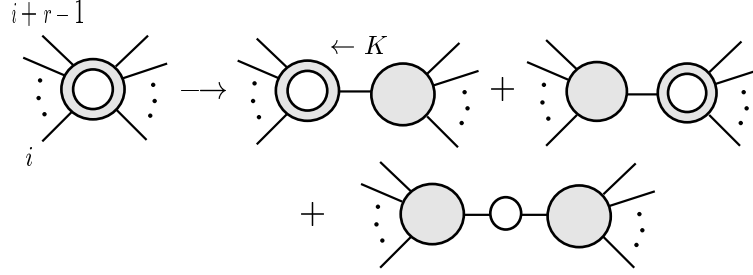


Figure 5. The diagrams with an explicit pole in  $K^2 = t_i^{[r]}$  coming from a tree propagator.

One of the results that we shall prove is that only a few integral functions may contribute to a pole in any multi-particle channel. Furthermore, the singular terms tightly constrain the coefficients of the allowed integral functions. The factorizing contributions in a multi-particle channel are composed only of integral functions depicted in fig. 6; all external momenta from one of the two sides of the multi-particle pole are part of one leg of these integral functions. If  $t_i^{[r]}$  constitutes a kinematic invariant of an entire leg of an integral function there will be non-factorization from the discontinuous limit. There are also two integral functions which may enter into non-factorization: the box functions  $I_{4:r-1;i+1}$  and  $I_{4:n-r-1;i+r+1}$  in fig. 7. (The values of these box functions are given in appendix IV.) These two box functions have the property that they contain explicit poles in  $K^2$  yet they would not appear in any of the naively factorized diagrams in fig. 5.

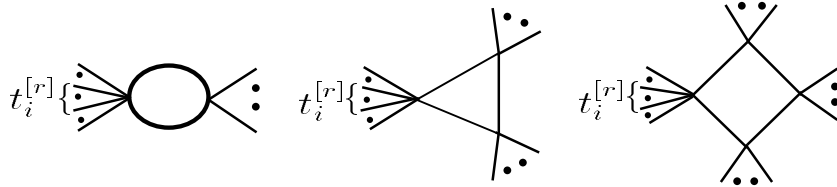


Figure 6. The integral functions which contribute to diagrams with a tree pole in the  $K^2 = t_i^{[r]}$  channel.

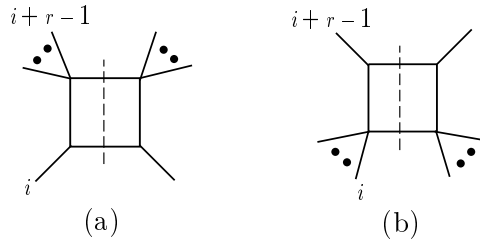


Figure 7. The two boxes functions which contribute to non-factorization in the channel  $t_i^{[r]}$ , indicated by the dashed line.

The procedure for obtaining the factorization function is similar to the one for obtaining the loop splitting functions. First compute the factorizing contribution given by the bubble loop in the third class of diagrams on the right-hand-side of figure 5. This contribution is of the form

$$C_1 \frac{1}{\epsilon} + C_0. \quad (4.3)$$



In this case there is no  $\epsilon^{-2}$  singularity since bubble diagrams have at worst  $\epsilon^{-1}$  ultraviolet singularities (in a Feynman-like gauge). Note that the bubble loop is gauge dependent. As was the case for two-particle factorization we must subtract an appropriate discontinuity function to obtain

$$C_1 \left[ \frac{1}{\epsilon} - b(t_i^{[r]}) \right] + C_0, \quad (4.4)$$

which is finite. After inserting a complete set of helicity states we obtain the factorizing contribution  $\mathcal{F}_n^{\text{fact}}$  from eq. (4.4). (In some cases, such as factorizing on a fermion line, this contribution vanishes.)

The second type of contribution to the factorization function,  $\mathcal{F}_n^{\text{non-fact}}$ , are the non-factorizing ones given in Table 2. The coefficients of the contributing terms in the third column are given in the first column. As for two-particle collinear limits the non-factorizing terms are fixed by the singular terms (2.6). The box functions  $F^{2mh}$  appearing in the third column of Table 2 are defined in eqs. (IV.10) and (IV.14) and correspond to the kinematic configurations depicted in fig. 7.

Coefficient	Singularity	Factorization Function Contribution
$\mathcal{S}_{i-1}^{[n]}$	$-\frac{1}{\epsilon^2} \left( \frac{\mu^2}{-s_{i-1,i}} \right)^\epsilon$	$2(\mu^2)^\epsilon \left( F_{n:r-1;i+1}^{2mh} + \frac{1}{\epsilon^2} (-t_i^{[r]})^{-\epsilon} \right)$
$\mathcal{S}_{i+r-1}^{[n]}$	$-\frac{1}{\epsilon^2} \left( \frac{\mu^2}{-s_{i+r-1,i+r}} \right)^\epsilon$	$2(\mu^2)^\epsilon \left( F_{n:n-r-1;i+r+1}^{2mh} + \frac{1}{\epsilon^2} (-t_i^{[r]})^{-\epsilon} \right)$
$\mathcal{C}^{[n]} - \mathcal{C}^{[n-1]}$	$\frac{1}{\epsilon}$	$(\mu^2)^\epsilon \frac{1}{\epsilon(1-2\epsilon)} (-t_i^{[r]})^{-\epsilon}$

**Table 2:** The ‘non-factorizing’ contributions to the factorization functions in the channel  $t_i^{[r]} \rightarrow 0$ . The three coefficients in the first column are the coefficients of the contributions to the factorization function given in the third column.

The total contribution to the factorization function  $\mathcal{F}_n$  is the sum of terms in Table 3 along with ones in eq. (4.4).

## 4.2 Multi-Particle Factorization Example

We now present an example to illustrate the use of multi-particle factorization to provide checks on explicitly calculated results. This is analogous to the types of checks that have been performed using collinear limits both for tree [27, 12] and loop [13,10,3] amplitudes. Multi-particle factorization can also be helpful for constructing ansätze for higher-point amplitudes.

Consider the one-loop  $N = 4$  supersymmetric six-gluon amplitude  $A_{6;1}^{N=4}(1^+, 2^+, 3^+, 4^-, 5^-, 6^-)$ , which has been computed in ref. [11]. In the  $t_1^{[3]} = (k_1 + k_2 + k_3)^2$  channel, the right-hand-side of eq. (4.1) vanishes since  $A^{\text{tree}}(1^+, 2^+, 3^+, K^\pm) = 0$ . Thus the amplitude does not contain a pole in  $t_1^{[3]}$ . The  $t_2^{[3]}$  channel, however, will contain a pole, since tree and loop amplitudes appearing on the right-hand-side of eq. (4.1) do not vanish. Since we are dealing with  $N = 4$  super-Yang-Mills, only box functions may enter [10] in the integral reduction. Therefore, the only integral functions which may contribute to the coefficient of the  $t_2^{[3]}$  pole are given by the four box functions  $F_{6:2}^{1m}, F_{6:5}^{1m}, F_{6:2;3}^{2mh}, F_{6:2;6}^{2mh}$ , which are depicted in fig. 8 and defined in eqs. (IV.10) and (IV.14). For

the first two integral functions the pole comes from a tree propagator, while for the second two integral functions the loop integral itself generates the pole. (The  $F$  functions have the kinematic poles scaled out, but the original integrals defined in eq. (IV.1) and related to the  $F$  in eq. (IV.15) contain them.)

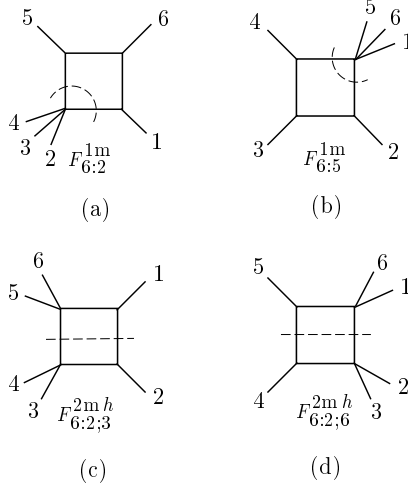


Figure 8. The four box functions which may appear as coefficients of a  $t_2^{[3]}$  pole in a six-point amplitude; the dashed lines represent the  $t_2^{[3]}$  channel.

For the  $N = 4$  supermultiplet with one gluon, four Weyl fermions and three complex scalars (with two states each) all ultraviolet and collinear singularities cancel leaving only the soft ones,

$$A_{6;1}^{N=4}(1^+, 2^+, 3^+, 4^-, 5^-, 6^-) \Big|_{\text{singular}} = -c_{\Gamma} A_6^{\text{tree}}(1^+, 2^+, 3^+, 4^-, 5^-, 6^-) \frac{1}{\epsilon^2} \sum_{j=1}^6 \left( \frac{\mu^2}{-s_{j,j+1}} \right)^\epsilon. \quad (4.5)$$

The tree amplitude in this equation contains a pole in the  $t_2^{[3]}$  channel given by

$$A_6^{\text{tree}}(1^+, 2^+, 3^+, 4^-, 5^-, 6^-) = A_4^{\text{tree}}(2^+, 3^+, 4^-, K^-) \frac{1}{t_2^{[3]}} A_4^{\text{tree}}(K^+, 5^-, 6^-, 1^+) + \text{non-pole}. \quad (4.6)$$

The four box functions which appear as coefficients of the  $t_2^{[3]}$  pole in the amplitude  $A_{6;1}^{N=4}$  have infrared singular behavior,

$$\begin{aligned} F_{6:2}^{1m} \Big|_{\text{singular}} &= -\frac{1}{\epsilon^2} \left[ (-s_{61})^{-\epsilon} + (-s_{56})^{-\epsilon} - (-t_2^{[3]})^{-\epsilon} \right], \\ F_{6:5}^{1m} \Big|_{\text{singular}} &= -\frac{1}{\epsilon^2} \left[ (-s_{34})^{-\epsilon} + (-s_{23})^{-\epsilon} - (-t_2^{[3]})^{-\epsilon} \right], \\ F_{6:2;3}^{2mh} \Big|_{\text{singular}} &= -\frac{1}{2\epsilon^2} \left[ (-s_{12})^{-\epsilon} + 2(-t_2^{[3]})^{-\epsilon} - (-s_{56})^{-\epsilon} - (-s_{34})^{-\epsilon} \right], \\ F_{6:2;6}^{2mh} \Big|_{\text{singular}} &= -\frac{1}{2\epsilon^2} \left[ (-s_{45})^{-\epsilon} + 2(-t_2^{[3]})^{-\epsilon} - (-s_{23})^{-\epsilon} - (-s_{61})^{-\epsilon} \right], \end{aligned} \quad (4.7)$$

and we have redundant constraints for determining their coefficients from eq. (4.5). This fixes the

relative coefficients of the four box functions to be unity so that

$$\begin{aligned}
A_{6;1}^{N=4}(1^+, 2^+, 3^+, 4^-, 5^-, 6^-) &= c_\Gamma \mu^{2\epsilon} A_4^{\text{tree}}(2^+, 3^+, 4^-, K^-) \frac{1}{t_2^{[3]}} A_4^{\text{tree}}(K^+, 5^-, 6^-, 1^+) \\
&\times 2 \left( F_{6;2}^{1m} + F_{6;5}^{1m} + F_{6;2;3}^{2mh} + F_{6;2;6}^{2mh} \right) + \text{non-pole},
\end{aligned} \tag{4.8}$$

where  $K = k_2 + k_3 + k_4$  and the tree amplitudes with the other helicity configuration of the intermediate line vanish. Thus, in the full amplitude, the  $t_2^{[3]}$  pole must multiply the four box functions in fig. 8 with a relative coefficient of unity.

From Table 2 we may also read off the factorization function in the  $t_2^{[3]}$  channel to be

$$\begin{aligned}
\mathcal{F}_6^{N=4}(t_2^{[3]}; k_1, \dots, k_6) &= 2(\mu^2)^\epsilon \left( F_{6;2;3}^{2mh} + F_{6;2;6}^{2mh} + \frac{2}{\epsilon^2} (-t_2^{[3]})^{-\epsilon} \right) \\
&= 2(\mu^2)^\epsilon \left[ -\frac{1}{\epsilon^2} \left[ (-s_{12})^{-\epsilon} - (-s_{56})^{-\epsilon} - (-s_{34})^{-\epsilon} \right] - \frac{1}{2\epsilon^2} \frac{(-s_{56})^{-\epsilon} (-s_{34})^{-\epsilon}}{(-s_{12})^{-\epsilon}} + \frac{1}{2} \ln^2 \left( \frac{s_{12}}{t_2^{[3]}} \right) \right. \\
&\quad \left. - \frac{1}{2} \ln^2 \left( \frac{s_{34}}{t_2^{[3]}} \right) - \frac{1}{2} \ln^2 \left( \frac{s_{56}}{t_2^{[3]}} \right) - \frac{\pi^2}{3} \right] + \{k_2 \leftrightarrow k_5, k_3 \leftrightarrow k_6, k_4 \leftrightarrow k_1\}.
\end{aligned} \tag{4.9}$$

Note that the integral functions do not undergo any particularly large simplification as  $t_2^{[3]} \rightarrow 0$ , in contrast to the simplification appearing in the splitting functions.

Finally, after explicitly taking the limit  $t_2^{[3]} \rightarrow 0$  we may rewrite eq. (4.8) as

$$\begin{aligned}
A_{6;1}^{N=4}(1^+, 2^+, 3^+, 4^-, 5^-, 6^-) &\longrightarrow c_\Gamma \mu^{2\epsilon} A_4^{\text{tree}}(2^+, 3^+, 4^-, K^-) \frac{1}{t_2^{[3]}} A_4^{\text{tree}}(K^+, 5^-, 6^-, 1^+) \\
&\times 2 \left( F^{0m}(k_2, k_3, k_4, K) + F^{0m}(K, k_5, k_6, k_1) + \mathcal{F}_6^{N=4} \right),
\end{aligned} \tag{4.10}$$

where the  $F^{0m}$  zero-external-mass box function is given in eq. (IV.10f). The three terms in eq. (4.10) correspond to the ones in eq. (4.1), after re-expressing the functions in terms of the four-point [35,10] loop amplitudes.

We may obtain the pole in the  $t_3^{[3]}$  channel by symmetry under reflection of the external states, so that the same results hold but with relabeled indices

$$A_{6;1}^{N=4}(1^+, 2^+, 3^+, 4^-, 5^-, 6^-) = c_\Gamma \mu^{2\epsilon} A_4^{\text{tree}} \frac{1}{t_3^{[3]}} A_4^{\text{tree}} \times 2 \left( F_{6;3}^{1m} + F_{6;6}^{1m} + F_{6;2;1}^{2mh} + F_{6;2;4}^{2mh} \right) + \text{non-pole}. \tag{4.11}$$

Now compare the results in eqs. (4.8) and (4.11) against the explicitly computed result of ref. [11]

$$A_{6;1}^{N=4}(1^+, 2^+, 3^+, 4^-, 5^-, 6^-) = c_\Gamma \left[ B_1 W_6^{(1)} + B_2 W_6^{(2)} + B_3 W_6^{(3)} \right], \tag{4.12}$$

where

$$\begin{aligned}
B_1 &= i \frac{([12] \langle 24 \rangle + [13] \langle 34 \rangle) ([31] \langle 16 \rangle + [32] \langle 26 \rangle) (t_1^{[3]})^3}{\langle 12 \rangle \langle 23 \rangle [45] [56] (t_1^{[3]} t_3^{[3]} - s_{12} s_{45}) (t_1^{[3]} t_2^{[3]} - s_{23} s_{56})}, \\
B_2 &= \left( \frac{\langle 1^+ | (k_2 + k_3) | 4^+ \rangle}{t_2^{[3]}} \right)^4 B_1|_{j \rightarrow j+1} + \left( \frac{[23] \langle 56 \rangle}{t_2^{[3]}} \right)^4 B_1^\dagger|_{j \rightarrow j+1}, \\
B_3 &= \left( \frac{\langle 3^+ | (k_1 + k_2) | 6^+ \rangle}{t_3^{[3]}} \right)^4 B_1|_{j \rightarrow j-1} + \left( \frac{[12] \langle 45 \rangle}{t_3^{[3]}} \right)^4 B_1^\dagger|_{j \rightarrow j-1},
\end{aligned} \tag{4.13}$$

and

$$W_6^{(i)} \equiv F_{6:i}^{1m} + F_{6:i+3}^{1m} + F_{6:2;i+1}^{2mh} + F_{6:2;i+4}^{2mh}. \tag{4.14}$$

The  $B_i^\dagger$  means complex conjugating spinor products in  $B_i$ ,  $\langle k j \rangle \leftrightarrow [j k]$  without complex conjugating factors of  $i$ , and the subscript  $j \rightarrow j + 1$  means applying a cyclic permutation of the six momenta  $k_i$ ,  $\{1, 2, 3, 4, 5, 6\} \rightarrow \{2, 3, 4, 5, 6, 1\}$ . The  $B_i$  satisfy the condition

$$B_1 + B_2 + B_3 = 2A_6^{\text{tree}}(1^+, 2^+, 3^+, 4^-, 5^-, 6^-). \tag{4.15}$$

The amplitude (4.12) clearly satisfies the multi-particle pole conditions described above: it does not contain a pole in the  $t_1^{[3]}$  channel and the coefficients of the  $t_2^{[3]}$  and  $t_3^{[3]}$  poles match the ones in eqs. (4.8) and (4.11). Thus the amplitude (4.13) is consistent with the constraints imposed by multi-particle factorization, providing a further stringent check on its correctness.

The same type of analysis may be performed for larger numbers of external legs. However, the singularities in  $\epsilon$  will not uniquely specify the coefficients of the boxes since the number of boxes proliferates. Nevertheless, all functions entering into the factorization function  $\mathcal{F}_n$  are uniquely specified from the singularities in  $\epsilon$ .

## 5. Proof of Universal Factorization

In this section we prove the factorization properties of amplitudes described in the two previous sections. Our proof is based on identifying all potential poles in a generic amplitude that arise either from tree propagators or within loop momentum integrals. We use the integral reduction procedure [36,37,38,39,40,23], reviewed (and slightly modified) in appendix I, to make the poles from loop integrals explicit. One might expect that all non-factorizing contributions should be related to the infrared divergences; our method of proof makes this connection explicit.

To summarize appendix I, any one-loop Feynman diagram may be expressed as a linear combination of integral functions with four or fewer legs multiplied by rational ‘reduction coefficients’. In the standard integral reduction procedure one obtains coefficients of integral functions which can contain dependence on  $\epsilon$ . Since we are linking all non-factorizing contributions to infrared singularities, any  $\epsilon$ -dependence would have to be tracked because it could induce finite shifts in the splitting and factorization functions when multiplying divergent integrals. Rather than dealing with  $\epsilon$ -dependent reduction coefficients, we find it simpler to keep all  $\epsilon$ -dependence in the basis

of integral functions. Thus, in the appendix we modify the usual reduction procedure in order to eliminate  $\epsilon$ -dependence in the reduction coefficients; through  $\mathcal{O}(\epsilon^0)$  this leads to the basis of integral functions: (a)  $D = 4 - 2\epsilon$  scalar bubbles, triangles and boxes, (b)  $D = 6 - 2\epsilon$  scalar bubbles and triangles, and (c)  $D = 8 - 2\epsilon$  scalar boxes. In the dimensional reduction or FDH schemes, where the number of states is always fixed at their four-dimensional value, there are no other sources of  $\epsilon$ -dependence. Thus, all amplitudes may be expressed as linear combinations of these integral functions with rational coefficients containing no  $\epsilon$ -dependence.

If the reduction coefficients contain poles or if the integral functions contain discontinuities or poles, the amplitudes may not factorize in a simple way. After having performed the integral reduction procedure on all Feynman diagrams contributing to an amplitude, poles in kinematic variables arise from three sources:<sup>†</sup>

- 1) diagrams which have a pole coming from an explicit tree propagator,
- 2) poles in the integral reduction coefficients, and
- 3) explicit poles appearing within the box and triangle integral functions in the basis.

The naively factorizing contributions are of the first type but all three can lead to non-factorization. We now systematically collect the non-factorizing pieces to the loop splitting function associated with each of the three types of kinematic poles. Subsequently, we will show that they are uniquely fixed by the singularities in  $\epsilon$  via eq. (2.6); this is because no non-zero linear combination can be constructed which is free of  $\epsilon^{-1}$ .

### 5.1 Kinematic Poles from Tree Propagators

Consider the Feynman diagrams containing a tree propagator which has a kinematic pole in the variable  $t_i^{[r]}$ , as depicted in fig. 5. In the limit that the kinematic variable vanishes one expects the amplitude to factorize on this pole since the diagrams break into a product of lower-point tree and loop amplitudes. However, if additional infrared divergences develop in the loop integrals as the kinematic invariant vanishes there will be discontinuities in the integral functions. In the off-shell case ( $t_i^{[r]} \neq 0$ ) there may be, for example, terms such as  $\ln(-t_i^{[r]})$  which correspond to poles in  $\epsilon$  in the on-shell case ( $t_i^{[r]} = 0$ ); in this case the off-shell to on-shell transition is discontinuous, and there is a ‘discontinuity function’ modifying the tree pole.

To find the non-factorizing contributions in the loop integrals of the diagrams in fig. 5 (including the case of collinear limits), we categorize all discontinuities in the integral functions (coming from the reduction) as the kinematic invariant  $K^2$  vanishes. (We denote momenta which are sums of external momenta  $k_i$  by an upper case letter; the lower case  $k_i$  we reserve for on-shell external momenta.) Out of all possible integral functions appearing after the reduction, discussed in appendix I, only those where one leg has momentum  $K$  have a discontinuous off-shell ( $K^2 \neq 0$ ) to on-shell ( $K^2 = 0$ ) transition. We now step through the possible discontinuities coming from these integrals, which are collected in appendix IV.

---

<sup>†</sup> We are assuming that the spinor helicity reference momenta are chosen so as to not introduce any additional poles in the channel of interest.

Consider first discontinuity functions arising from the  $D = 4 - 2\epsilon$  bubble function. Since bubbles are a function of a single momentum, the only ones which can have a non-smooth limit as  $K^2 \rightarrow 0$  are those with momentum  $K$  flowing through them. Bubble integrals with on-shell (massless) legs vanish by a standard dimensional regularization prescription [31], so the off-shell bubble (IV.2) is itself a discontinuity function. Thus we have the discontinuity function given by

$$b(K^2) = \frac{1}{r_\Gamma} I_2[1](K^2) = \frac{1}{\epsilon(1-2\epsilon)} (-K^2)^{-\epsilon}, \quad (5.1)$$

where  $r_\Gamma$  is the ratio of Gamma-functions in eq. (IV.3).

Consider now the discontinuity functions arising from the  $D = 4 - 2\epsilon$  triangle integrals, depicted in fig. 9. Starting from the three-external-mass integral, depicted in fig. 9a and explicitly defined in eqs. (IV.7a) and (IV.4a), and taking  $K_3^2 \rightarrow 0$  one obtains

$$T_3^{3m}(K_1^2, K_2^2, K_3^2) \longrightarrow T_3^{2m}(K_1^2, K_2^2) - d_2(K_3^2; K_1^2, K_2^2) + d_2(K_3^2; K_2^2, K_1^2), \quad (5.2)$$

where  $T_3^{2m}$  is the two-external-mass triangle depicted in fig. 9b and explicitly given in eqs. (IV.7b) and (IV.4b). Equation (5.2) defines the discontinuity function  $d_2$  to any finite order in  $\epsilon$ . Through  $\mathcal{O}(\epsilon^0)$ , it is

$$d_2(K_3^2; K_1^2, K_2^2) \equiv \frac{1}{2\epsilon^2} (-K_3^2)^{-\epsilon} - \frac{1}{2\epsilon^2} \frac{(-K_3^2)^{-\epsilon} (-K_1^2)^{-\epsilon}}{(-K_2^2)^{-\epsilon}} - \text{Li}_2\left(1 - \frac{K_1^2}{K_2^2}\right), \quad (5.3)$$

and satisfies the property

$$d_2(K_3^2; K_1^2, K_2^2) = -d_2(K_3^2; K_2^2, K_1^2), \quad (5.4)$$

as may be checked using the dilogarithm identity

$$\text{Li}_2(1-x) + \text{Li}_2(1-x^{-1}) = -\frac{1}{2} \ln^2(x). \quad (5.5)$$

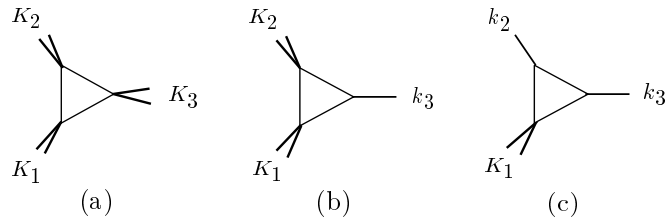


Figure 9. The triangle functions generate two types of discontinuity function as one of the external legs becomes on-shell (or massless).

Next, by taking  $K_2^2 \rightarrow 0$  the two-external-mass scalar triangle in fig. 9b becomes

$$\begin{aligned} T_3^{2m}(K_1^2, K_2^2) &\longrightarrow \left[ \frac{1}{\epsilon^2} (-K_1^2)^{-\epsilon} - \frac{1}{\epsilon^2} (-K_2^2)^{-\epsilon} \right] \\ &= T_3^{1m}(K_1^2) - d_1(K_2^2), \end{aligned} \quad (5.6)$$

where the discontinuity function is

$$d_1(K^2) \equiv \frac{1}{\epsilon^2} (-K^2)^{-\epsilon}. \quad (5.7)$$

Finally, by taking  $K_1^2 \rightarrow 0$  for the one-external-mass triangle depicted in fig. 9c we obtain

$$T_3^{1m}(K_1^2) = d_1(K_1^2). \quad (5.8)$$

Note that the zero-external-mass triangle vanishes.

Now consider discontinuities in the  $D = 4 - 2\epsilon$  box. These are readily obtainable from the general relationship between box and triangle functions [40]

$$I_4[1] = \frac{1}{2} \left[ \sum_{i=1}^4 c_i I_3^{(i)}[1] + (-1 + 2\epsilon) c_0 I_4^{D=6-2\epsilon}[1] \right], \quad (5.9)$$

where

$$c_i = \sum_{j=1}^4 S_{ij}^{-1}, \quad c_0 = \sum_{i=1}^4 c_i = \sum_{i,j=1}^4 S_{ij}^{-1}, \quad S_{ij} = -\frac{1}{2} (p_{i-1} - p_{j-1})^2. \quad (5.10)$$

Here  $p_i = \sum_{j=1}^i K_j$ , where the  $K_j$  are the external momenta of the box functions and  $p_0 = 0$ .

The six-dimensional box function  $I_4^{D=6-2\epsilon}[1]$  in eq. (5.9) (expanded to a finite order around  $\epsilon = 0$ ) has a smooth transition between external massive and massless kinematics since it does not contain infrared divergences and the loop integral converges uniformly. Thus from eq. (5.9), the only discontinuity functions that may appear in box functions are linear combinations of ones appearing for triangle functions (5.7) and (5.3) (and explicitly listed in Table 5 in section 6) and there is no need for a separate analysis.

Finally, consider the higher-dimensional integrals. These higher dimension boxes, triangles and bubbles arise from the reduction of tensor integrals, following the procedure discussed in appendix I. (If one were keeping terms of  $\mathcal{O}(\epsilon)$  and beyond, then the basis is further enlarged to include higher-dimensional integrals with  $n \geq 5$  legs.) In general, these integrals are smooth as an external leg makes an off- to on-shell transition since no infrared divergences develop. Therefore they will not contribute a discontinuity function. There are, however, two exceptions which need a closer examination:

$$I_2^{D=6-2\epsilon}[1](K^2) = -\frac{r_\Gamma}{2\epsilon(1-2\epsilon)(3-2\epsilon)} (-K^2)^{1-\epsilon}, \quad (5.11)$$

$$I_3^{1m, D=6-2\epsilon}[1](K^2) = \frac{r_\Gamma}{2\epsilon(1-\epsilon)(1-2\epsilon)} (-K^2)^{-\epsilon}.$$

These integral functions are proportional to  $I_2$  in eq. (5.1), but with  $\epsilon$ -dependent coefficients. The possibility of the integrals (5.11) contributing to non-factorization would be problematic since their difference is simply a constant, which would not be linked to a singularity in  $\epsilon$ . In appendix III we show that the integrals in eq. (5.11) do not contribute for  $K^2 \rightarrow 0$ , leaving only  $D = 4 - 2\epsilon$

integrals as source of discontinuity functions; there are no additional discontinuity functions from any of the higher-dimensional integrals.

Converting to the  $n$ -point kinematic variables in the  $K^2 = t_i^{[r]} \rightarrow 0$  channel, the discontinuity functions which may enter from the loop diagrams in fig. 5 are thus

$$\begin{aligned} d_1(t_i^{[r]}) &= \frac{1}{\epsilon^2} (-t_i^{[r]})^{-\epsilon}, \\ d_2(t_i^{[r]}; t_{i+r}^{[r']}, t_i^{[r+r']}) &= \frac{1}{2\epsilon^2} (-t_i^{[r]})^{-\epsilon} - \frac{1}{2\epsilon^2} \frac{(-t_i^{[r]})^{-\epsilon} (-t_{i+r}^{[r']})^{-\epsilon}}{(-t_i^{[r+r']})^{-\epsilon}} - \text{Li}_2\left(1 - \frac{t_{i+r}^{[r']}}{t_i^{[r+r']}}\right), \\ b(t_i^{[r]}) &= \frac{1}{\epsilon(1-2\epsilon)} (-t_i^{[r]})^{-\epsilon}, \end{aligned} \quad (5.12)$$

where  $2 \leq r' \leq n - r - 2$ . These discontinuity functions describe the additional contributions one would find from diagrams containing a tree propagator pole in  $t_i^{[r]}$ . For example, as  $K^2 = t_i^{[r]} \rightarrow 0$ , the first set of diagrams on the right-hand-side of fig. 5 behave as

$$\sum_{\lambda=\pm} A_{r+1}^{\text{loop}}(\dots, K^\lambda) \frac{1}{K^2} A_{n-r+1}^{\text{tree}}(K^{-\lambda}, \dots) + \frac{1}{K^2} \sum \text{discontinuities}, \quad (5.13)$$

where the discontinuities are the ones in eq. (5.12) multiplying rational coefficients (determined in section 5.4) where the pole in  $K^2$  comes from the intermediate tree propagator. That is, the diagrams factorize as one might naively expect, except that there are possible additional discontinuity contributions multiplying the explicit tree pole.

The origin of the discontinuities in eq. (5.12) may be traced back to the implicit expansion of amplitudes in  $\epsilon$ ; if one were to keep the full functional behavior in  $\epsilon$  there would be no discontinuity for  $\epsilon < 0$  since they can be analytically continued to zero. Note that the discontinuity functions contain non-singular (in  $\epsilon$ ) contributions, including the dilogarithm; these finite contributions are linked to the infrared singular ones because they are part of a single function.

## 5.2 Kinematic Poles from Integral Reduction Coefficients

As discussed in appendix II poles may appear in the reduction coefficients as two external momenta become collinear (or as an external momentum becomes soft) and not in multi-particle channels for general kinematics (except for the tensor bubble (I.20) which generates a multi-particle pole that is canceled by the  $D = 6 - 2\epsilon$  bubble). For convenience we choose the  $s_{12}$  channel. Only loop diagrams of the type in fig. 10 may generate potential  $s_{12}$  poles in the reduction coefficients. (For gluon amplitudes with scalar loops these types of diagrams were explicitly analyzed in refs. [13,15].) We will present a general argument and analysis that all such poles are proportional to the discontinuity functions (5.12).

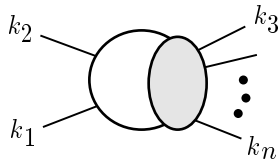


Figure 10. The class of loop integral which may generate a pole in  $s_{12}$ .



For the case of loop integrals which have a uniform non-vanishing mass in the loop (see eq. I.1), it is a simple matter to argue directly from the loop momentum representation that there are no massless poles. The mass acts as an infrared cutoff which prevents the integral from diverging as a kinematic variable vanishes. Alternatively, in the integral reduction framework, the reduction coefficients explicitly given in appendix I do appear to contain the poles collected in appendix II; for the case of a uniform mass in the loop these poles are necessarily spurious (i.e., the residue vanishes) since massive loop integrals cannot contain massless poles. (The spurious nature of these poles was first noted by Brown [36].) The specific details of how the residues of poles in the reduction coefficients all vanish is in general quite intricate and may involve Abel's [41] dilogarithm identity; nevertheless they must vanish.

As shown in appendix II, the reduction coefficients for the case of a uniform mass in the loop contain exactly the same apparent poles as for the massless case. In the massive loop case the residue of all massless poles cancel so one might expect the residues to also vanish for a massless loop. Indeed by taking the massive loop integral residues (which vanish) and taking  $m \rightarrow 0$  one obviously still obtains zero since the limit is smooth; all potential non-smoothness would be of the form  $\ln(m)$ , but such terms (as well as all others in the residue) vanish.

We must, however, be a bit more careful for the massless case since we must take the limits in the reverse ordering: first we set  $m = 0$  and then we extract the residue of the kinematic pole. After setting the internal mass to zero, the extraction of the residue by taking the appropriate kinematic variable to vanish may no longer be smooth since new infrared divergences may develop. The new singularities can prevent the necessary identities for the vanishing of the residues in the massive case from holding. Thus we need to collect the new singularities and all associated discontinuities from the integral functions. This situation is completely identical to the case where the pole arises from a tree propagator. The analysis is completely identical and the non-smooth behavior of any integral function when a kinematic variable vanishes is described by the discontinuity functions (5.12). Thus any (non-spurious) poles in the reduction coefficients must give a contribution to splitting or factorization functions proportional to discontinuity functions.

We have performed a number of explicit checks to verify the above general argument. Consider for example the scalar pentagon integrals with the kinematic configuration depicted in fig. 11, where momenta  $k_1$  and  $k_2$  are on-shell and the remaining  $K_i$  are either on-shell or off-shell. As discussed in appendix II, for this kinematic configuration the reduction coefficients contain poles in  $s_{12}$ .

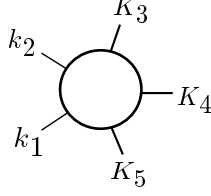


Figure 11. The original  $n$ -point integral may be reduced into a sum of pentagons; the type of pentagon depicted here is the only one which can generate poles in  $s_{12}$ .

From the discussion in appendix I, the pentagon integrals are

$$I_5 = \frac{1}{2} \sum_{i=1}^5 c_i I_4^{(i)} + \epsilon c_0 I_5^{D=6-2\epsilon}, \quad (5.14)$$

where

$$c_i = \sum_{j=1}^5 S_{ij}^{-1}, \quad c_0 = \sum_{i=1}^5 c_i, \quad S_{ij} = -\frac{1}{2}(p_{i-1} - p_{j-1})^2. \quad (5.15)$$

For on-shell  $k_1$  and  $k_2$  it is straightforward to check that as  $s_{12} \rightarrow 0$

$$S_{ij}^{-1} \longrightarrow (-1)^{i+j+1} \frac{1}{s_{12}} \frac{\sqrt{\det S^{(i)}} \sqrt{\det S^{(j)}}}{\sqrt{\det S^{(1)}} \sqrt{\det S^{(3)}}} + \mathcal{O}(1), \quad (5.16)$$

where

$$\begin{aligned} 4\sqrt{\det S^{(1)}} &= s_{23}s_{34} - s_{51}K_3^2, & 4\sqrt{\det S^{(2)}} &= s_{34}s_{45} - K_3^2K_5^2, \\ 4\sqrt{\det S^{(3)}} &= s_{45}s_{51} - s_{23}K_5^2, & 4\sqrt{\det S^{(4)}} &= s_{51}s_{12}, \\ 4\sqrt{\det S^{(5)}} &= s_{12}s_{23}. \end{aligned} \quad (5.17)$$

The  $S_{mn}^{(i)}$  are the matrices for the daughter box diagram obtained by removing the internal propagator between leg  $(i-1)$  and leg  $i$ . (This follows the same labeling convention as for the box diagrams themselves.) Since  $\sqrt{\det S^{(4)}}$  and  $\sqrt{\det S^{(5)}}$  are both proportional to  $s_{12}$ , only the three coefficients  $c_1, c_2$  and  $c_3$  contain a pole in  $s_{12}$  and are relevant.

In all cases, the coefficients  $c_4$  and  $c_5$  do not contain any singularities. Rather, the integrals  $I_4^{(4)}$  and  $I_4^{(5)}$  themselves contain a divergence. Since we are only investigating the singular behavior of the reduction coefficients, we only consider the partial sum over  $c_1, c_2$ , and  $c_3$

$$c_1 I_4^{(1)} + c_2 I_4^{(2)} + c_3 I_4^{(3)} = -\frac{r_\Gamma}{2} \frac{1}{s_{12}} \frac{1}{\sqrt{\det S^{(1)}} \sqrt{\det S^{(3)}}} \left( \sum_{j=1}^5 (-1)^j \sqrt{\det S^{(j)}} \right) \left( F_4^{(1)} - F_4^{(2)} + F_4^{(3)} \right), \quad (5.18)$$

where we used eq. (IV.8) to scale out the overall kinematic denominator from each integral function.

As explained above, for any configuration of  $K_3, K_4$  and  $K_5$ , being massive ( $K_i^2 \neq 0$ ) or massless ( $K_i^2 = 0$ ) we have

$$\lim_{k_1 \parallel k_2} (F_4^{(1)} - F_4^{(2)} + F_4^{(3)}) = \alpha d_1(s_{12}) + \beta d_2(s_{12}; K_3^2, s_{45}) + \gamma d_2(s_{12}; K_5^2, s_{34}), \quad (5.19)$$

where the  $\alpha, \beta$  and  $\gamma$  are constants. The combination of box functions  $F_4^{(1)}$ ,  $F_4^{(2)}$ , and  $F_4^{(3)}$  is displayed in fig. 12. We have explicitly verified through  $\mathcal{O}(\epsilon^0)$  that this holds for all possible kinematic configurations. For each situation the real numbers  $\alpha, \beta$ , and  $\gamma$  were found by explicitly performing the limit for all types of box integrals (i.e. for the different cases of whether or not  $K_3^2 = 0$ ,  $K_4^2 = 0$ , or  $K_5^2 = 0$ ). In all cases the discontinuity functions come from  $F_4^{(2)}$ , which is the only one of the three box functions which acquires new infrared singularities as  $s_{12} \rightarrow 0$ . (See table 5 in section 6 for a list of all box discontinuities.) The identity (5.19) is quite non-trivial when actually performing the limit on the integrals in appendix IV since many dilogarithm identities must be used in the process. Nevertheless, in a theory with a mass such identities necessarily exist to cancel the pole in the reduction coefficients; in the massless limit these identities break down in the infrared, leaving behind discontinuity functions containing singularities in  $\epsilon$ .

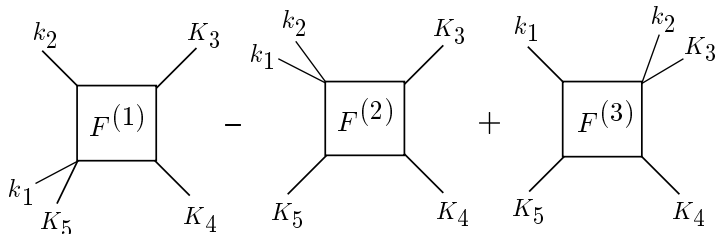


Figure 12. An example of a non-trivial identity in the collinear limit  $k_1 \parallel k_2$  is that this sum of box functions reduces to discontinuity functions;  $k_1$  and  $k_2$  are on-shell while  $K_3, K_4$  and  $K_5$  are either on- or off-shell.

As a second check, the general five-point integral with one power of loop momenta is [40,23]

$$I_5[l^\mu] = \sum_{i=i}^4 p_i^\mu \sum_{j=1}^5 S_{i+1,j}^{-1} I_4^{(j)} \xrightarrow{k_1 \parallel k_2} \frac{r_\Gamma}{2} \sum_{i=2}^5 p_i^\mu (-1)^{i+1} \frac{\sqrt{\det S^{(i+1)}}}{s_{12} \sqrt{\det S^{(1)}} \sqrt{\det S^{(3)}}} \sum_{j=1}^3 (-1)^j F_4^{(j)}, \quad (5.20)$$

so once again identity (5.19) guarantees that any pole in  $s_{12}$  is proportional to a linear combination of discontinuity functions. One can continue in this way to show that any poles in  $s_{12}$  are proportional to linear combinations of discontinuity functions even for higher powers of loop momentum in the numerator. We have also verified that the poles in the reduction coefficients of scalar hexagons are also proportional to discontinuity functions.

The explicit reduction results above are complete for an  $N = 4$  supersymmetric theory since the only integrals encountered [10] that can produce a collinear pole in reduction coefficients (using the reduction basis discussed in appendix II) are the ones discussed above. A proof of the lack of collinear poles in integrals for the case of external gluons with scalar and fermion loops has previously been constructed by a direct diagrammatic analysis [13,15]. Since gluon loops may be interpreted in terms of a linear combination of scalar, fermion and  $N = 4$  loops [1,42], this provides a complete check of our general argument for  $n$ -gluon amplitudes.

In summary, all contributions with a kinematic pole in the reduction coefficients are proportional to

$$\sum \text{discontinuities}, \quad (5.21)$$

where the discontinuities are again the ones in eq. (5.12). The general argument we have presented above holds for any type of massless pole. Besides collinear poles, the reduction coefficients may contain poles as momenta become soft or ones not found in amplitudes, such as in non-adjacent kinematic variables (e.g.  $s_{13}$ ); in view of the above general argument all such poles must either be spurious or proportional to discontinuity functions.

### 5.3 Kinematic Poles from Integral Functions

The third source of kinematic poles are in the explicit forms of the integral functions contained in the reduction basis. In eqs. (IV.7) and (IV.15) of appendix IV overall dimensions have been explicitly pulled out from the  $D = 4 - 2\epsilon$  scalar integral functions; the only ones that have kinematic poles in two- or multi-particle channel are  $I_3^{1m}$ ,  $I_4^{1m}$  and  $I_4^{2mh}$ . In a two-particle channel  $s_{i,i+1}$  the integral functions

$$\begin{aligned}
I_{4:i+2}^{1m} &\equiv -\frac{2r_\Gamma}{s_{i,i+1}s_{i-1,i}} F_{n:i+2}^{1m}, & I_{4:i+3}^{1m} &\equiv -\frac{2r_\Gamma}{s_{i,i+1}s_{i+1,i+2}} F_{n:i+3}^{1m}, \\
I_{4:r;i+2}^{2mh} &\equiv -\frac{2r_\Gamma}{s_{i,i+1}t_{i+1}^{[r+1]}} F_{n:r;i+2}^{2mh}, & I_{3:i}^{1m} &\equiv -\frac{r_\Gamma}{s_{i,i+1}} T_{n:i}^{1m} = -\frac{r_\Gamma}{s_{i,i+1}} d_1(s_{i,i+1}),
\end{aligned} \tag{5.22}$$

contain poles, which are depicted in fig. 13. These integrals arise from the reduction of the type of diagrams in fig. 10. All other scalar integrals in the basis do not diverge as  $s_{i,i+1} \rightarrow 0$ . We also note that the triangle function  $T_{n:i}^{1m}$  is equal to the discontinuity function  $d_1(s_{i,i+1})$  defined in eq. (5.7).

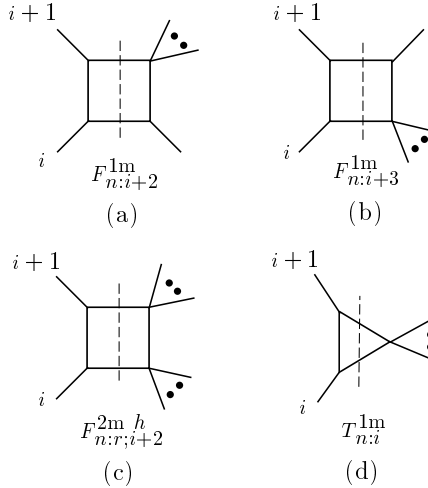


Figure 13. The integral functions which have a pole in  $s_{i,i+1}$ .

The case of multi-particle poles is similar, and only the two integrals (depicted in fig. 7)

$$I_{4:r-1;i+1}^{2mh} = \frac{-2r_\Gamma}{t_{i-1}^{[2]} t_i^{[r]}} F_{n:r-1;i+1}^{2mh}, \quad I_{4:n-r-1;i+r+1}^{2mh} = \frac{-2r_\Gamma}{t_{i+r-1}^{[2]} t_i^{[r]}} F_{n:n-r-1;i+r+1}^{2mh}, \tag{5.23}$$

contain poles in the channel  $t_i^{[r]}$  ( $r > 2$ ).

Finally there are the higher-dimension integrals. Such integrals, however, cannot contain (non-spurious) poles. In general the nearest neighbor  $t_i^{[r]}$  poles in the integrals come from isolated regions in the loop momentum integral. In six- or higher-dimensions the measure  $d^D l$  prevents the occurrence of a pole from the dominant region of the loop momentum integral, where propagators become singular. This type of analysis is similar to the previously performed analysis of the suppression of poles in  $n$ -gluon diagrams containing internal scalars [13,15].

#### 5.4 Linking all contributions to singularities

Having found all possible non-factorizing forms containing poles in the channel of interest, we now go on to fix their coefficients by requiring that the singular terms are consistent with the known behavior in eq. (2.6).

First consider two-particle collinear limits. The loop diagrams in fig. 2, containing the factorizing contributions to the loop splitting functions, may contain singularities in  $\epsilon$  which depend on the details (and gauge choices) of the process under discussion. A procedure which simplifies our discussion is to collect all singularities in the non-factorizing set. We therefore always subtract and add the discontinuity functions  $b(s_{i,i+1})$  and  $d_1(s_{i,i+1})$  given in eq. (5.12) with coefficients adjusted to move the singularities to the non-factorizing contributions. (See section 3.2 for an explicit example of this procedure.)

In Table 3 we collect all non-factorizing contributions to  $\text{Split}^{\text{loop}}$  in eq. (3.1), along with the singular terms which we use to fix the coefficients. These singular terms satisfy the property that there is no non-zero linear combination which is free of poles in  $\epsilon$ . Since all singular terms appearing in one-loop amplitudes are necessarily proportional to tree amplitudes, the final non-factorizing part of the loop splitting functions must be proportional to tree-level splitting functions, as given in eq. (3.9).

To fix the coefficients we systematically step through Table 3. Starting with the first row we have the potential contribution to  $\text{Split}^{\text{loop}}$ ,

$$F_{n:i+2}^{\text{lm}} \xrightarrow{k_i \| k_{i+1}} -\frac{1}{\epsilon^2} \left( -z s_{i,i+1} \right)^{-\epsilon} - \text{Li}_2(1-z) + \mathcal{O}(\epsilon), \quad (5.24)$$

which is the only non-factorizing function containing a  $\ln(z)/\epsilon$ . We may fix the coefficient of this term by comparing it to the coefficient of the same term in the original  $n$ -point amplitude, on the left-hand-side of eq. (3.1). In the collinear limit where  $k_i = zK$  and  $k_{i+1} = (1-z)K$ , from eq. (2.6), we have

$$-c_\Gamma \mathcal{S}_{i-1}^{[n]} \frac{1}{\epsilon^2} \left( \frac{\mu^2}{-s_{i-1,i}} \right)^\epsilon A_n^{\text{tree}} \xrightarrow{k_i \| k_{i+1}} -c_\Gamma \mathcal{S}_{i-1}^{[n]} \left[ \frac{1}{\epsilon^2} + \frac{1}{\epsilon} \ln \left( \frac{\mu^2}{-s_{i-1,K}} \right) - \frac{1}{\epsilon} \ln(z) \right] \sum_{\lambda=\pm} \text{Split}^{\text{tree}} A_{n-1}^{\text{tree}} + \mathcal{O}(\epsilon^0), \quad (5.25)$$

where  $s_{i-1,K} = (k_{i-1} + K)^2$ . This is the only singular term in the original  $n$ -point amplitude containing a  $\ln(z)/\epsilon$  in the collinear limit.

Potential Contribution	Selected Singular Part	Collinear Limit
$F_{n:i+2}^{1m}$	$\frac{1}{\epsilon} \ln(-s_{i-1,i})$	$\frac{1}{\epsilon} \ln(-zs_{i-1,K})$
$F_{n:i+3}^{1m}$	$\frac{1}{\epsilon} \ln(-s_{i+1,i+2})$	$\frac{1}{\epsilon} \ln(-(1-z)s_{K,i+2})$
$F_{n:r;i+2}^{2mh}$	$\frac{1}{\epsilon} \ln(-t_{i+1}^{[r+1]})$	$\frac{1}{\epsilon} \ln(-(1-z)t_K^{[r+1]} - zt_{i+2}^{[r]})$
$d_2(s_{i,i+1}; t_{i+2}^{[r]}, t_i^{[r+2]})$	$-\frac{1}{2\epsilon} \ln(-t_{i+2}^{[r]}/t_i^{[r+2]})$	$-\frac{1}{2\epsilon} \ln(-t_{i+2}^{[r]}/t_K^{[r+1]})$
$d_1(s_{i,i+1})$	$\frac{1}{\epsilon} \ln(-s_{i,i+1})$	$\frac{1}{\epsilon} \ln(-s_{i,i+1})$
$b(s_{i,i+1})$	$\frac{1}{\epsilon}$	$\frac{1}{\epsilon}$

**Table 3:** Particular singular terms in the second column used to fix the coefficients of potential non-factorizing contributions to  $\text{Split}^{\text{loop}}$ .

Matching the coefficients of the  $\ln(z)/\epsilon$  in the potential contribution (5.24) to the one in the  $n$ -point amplitude (5.25) gives the splitting function contribution

$$c_\Gamma \mathcal{S}_{i-1}^{[n]} \text{Split}^{\text{tree}} \left( d_1(s_{i,i+1}) + \mu^{2\epsilon} F_{n:i+2}^{1m} \Big|_{k_i \parallel k_{i+1}} \right), \quad (5.26)$$

which is thus fixed by the coefficient  $\mathcal{S}_{i-1}^{[n]}$  in the original  $n$ -point amplitude. Since  $F_{n:i+2}^{1m}$  also contains a  $\ln(-s_{i,i+1})/\epsilon$  it is convenient to subtract out this singularity using the discontinuity function  $d_1(s_{i,i+1})$ , so that we only adjust the coefficient of one singularity at a time. In the collinear limit the singular term (5.25) in the amplitude also contains a  $\ln(-s_{i-1,K})/\epsilon$  which exactly matches a corresponding singularity in the loop amplitude  $A_{n-1}^{\text{loop}}$  on the right-hand-side of eq. (3.1). Pulling out the pre-factor  $c_\Gamma \text{Split}^{\text{tree}}$ , as in eq. (3.9), gives the first term in eq. (3.10). The collinear limit  $k_i \parallel k_{i+1}$  of eq. (5.26) gives the first entry of Table 1.

Following similar reasoning, the coefficient of  $\ln(1-z)/\epsilon$  in the amplitude matches the one in the splitting function

$$c_\Gamma \mathcal{S}_{i+1}^{[n]} \text{Split}^{\text{tree}} \left( d_1(s_{i,i+1}) + \mu^{2\epsilon} F_{n:i+3}^{1m} \Big|_{k_i \parallel k_{i+1}} \right), \quad (5.27)$$

where

$$F_{n:i+3}^{1m} \xrightarrow{k_i \parallel k_{i+1}} -\frac{1}{\epsilon^2} \left( -(1-z)s_{i,i+1} \right)^{-\epsilon} - \text{Li}_2(z) + \mathcal{O}(\epsilon). \quad (5.28)$$

The contribution (5.27) corresponds to the the second entry in the third column of Table 2.

The third and fourth rows in Table 3 contain singular terms which are nowhere to be found in  $n$ -point amplitudes or in the factorizing portion, so the coefficients must vanish, explaining the absence of such contributions in Table 1.

Since we have collected all  $\ln(-s_{i,i+1})/\epsilon$  singularities together by moving such terms from the factorizing diagrams to the non-factorizing contributions, the coefficient of the  $d_1(s_{i,i+1})$  contribution is simply  $\mathcal{S}_i^{[n]}$  to match the same singularity in the amplitude, as given in the third row of Table 1. Finally, the coefficient of  $b(s_{i,i+1})$ , which is the only contribution to the splitting function containing a  $1/\epsilon$  singularity (without a logarithm), is determined by the difference of the coefficients  $\mathcal{C}^{[n]}$  for the  $n$ -point amplitude and  $\mathcal{C}^{[n-1]}$  for the  $(n-1)$ -point amplitude.

Now consider factorization in a multi-particle channel  $t_i^{[r]} \rightarrow 0$ . The procedure for adjusting the coefficients of potential contributions to the factorization functions is similar to the two-particle collinear case. Once again the non-factorizing contributions must be proportional to a product of factorized trees, because the singularities in  $\epsilon$  are necessarily of this form. Following the same logic the reader may step through the rows of Table 4 to obtain the entries in Table 2.

Potential Contribution	Selected Singular Part
$F_{n:r-1;i+1}^{2mh}$	$\frac{1}{\epsilon} \ln(-s_{i-1,i})$
$F_{n:n-r-1;i+r+1}^{2mh}$	$\frac{1}{\epsilon} \ln(-s_{i+r-1,i+r})$
$d_2(t_i^{[r]}; t_{i+r}^{[r']}, t_i^{[r+r']})$	$-\frac{1}{2\epsilon} \ln(-t_{i+r}^{[r']}/t_i^{[r+r']})$
$d_1(t_i^{[r]})$	$\frac{1}{\epsilon} \ln(-t_i^{[r]})$
$b(t_i^{[r]})$	$\frac{1}{\epsilon}$

**Table 4:** Selected singular terms associated with integrals with potential non-factorizing contribution in the multi-particle  $t_i^{[r]}$  channel.

Thus we have fixed the coefficients of all non-factorizing contributions in eqs. (3.1) and (4.1) for  $\text{Split}^{\text{loop}}$  and  $\mathcal{F}_n$  and established the rules in Tables 1 and 2. The discussion we have presented here is valid to any order in  $\epsilon$ ; the only modification being that the box functions appearing in these tables be kept to higher order.

## 6. Discontinuity Functions as a Tool for Evaluating Integrals

In this section we illustrate the use of discontinuity functions as a tool for obtaining infrared divergent box integrals from known infrared finite ones.

The infrared finite scalar box integrals of ref. [22] were evaluated in four dimensions. In ref. [23] a separate analysis for the infrared divergent integrals was performed due to the need for dimensionally regularized expressions. Since the discontinuity functions summarize the transition between infrared finite and infrared divergent integrals this suggests a procedure for obtaining infrared divergent scalar box integrals directly from infrared finite ones. After subtracting off the discontinuity function one simply takes the appropriate mass or kinematic invariants to vanish to

obtain the desired integrals. This procedure is made practical by eq. (5.9) which gives the necessary box discontinuity functions from the much simpler triangle functions. Thus, using known infrared finite box integrals, any infrared divergent box integral is reduced to an evaluation of simpler triangle integrals.

To illustrate the method we reproduce all the infrared divergent box integrals (depicted in fig. 14) necessary for computations in massless theories given in ref. [23]. Starting with the four-mass box one takes the limit of a vanishing external kinematic invariant (or mass) and subtracts the appropriate discontinuity function. For example, to obtain the three-external-mass integral (fig. 14b) from the four-external-mass integral (fig. 14a) given in ref. [22] we have from the first row of Table 5,

$$\lim_{K_1^2 \rightarrow 0} \left[ F^{4m}(K_1, K_2, K_3, K_4) - d_2(K_1^2; K_2^2, (K_1+K_2)^2) - d_2(K_1^2; K_4^2, (K_4+K_1)^2) \right] = F^{3m}(k_1, K_2, K_3, K_4). \quad (6.1)$$

This result agrees with the explicitly calculated result in ref. [23]. The reader may verify that all other infrared divergent box functions derived in ref. [23] may be obtained in this way, by using the discontinuity functions collected in table 5.\*

This method for obtaining box integrals may be used for any of the infrared divergent one-loop box integrals. In particular, box integrals with mixed massive and massless internal and/or external legs may also be obtained efficiently in this way. This method might also be useful for higher-loop integrals, but one would need a method for obtaining discontinuity functions that were obtained at one loop through eq. (5.9).

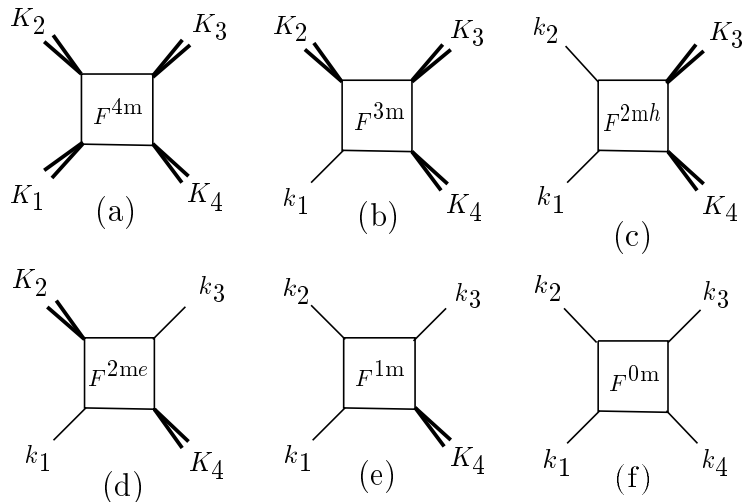


Figure 14. The box functions appearing in Table 5; the upper-case  $K_i$  represent off-shell ( $K_i^2 \neq 0$ ) and lower-case  $k_i$  represent on-shell momenta.

---

\* In ref. [23] sign errors were inadvertently introduced in the four-external-mass box integral obtained from ref. [22]; these signs are corrected in ref. [11].



Integral Functions	Limit	Discontinuity
$F^{4m} \rightarrow F^{3m}$	$K_1^2 \rightarrow 0$	$d_2(K_1^2; K_2^2, (K_1 + K_2)^2) + d_2(K_1^2; K_4^2, (K_4 + K_1)^2)$
$F^{3m} \rightarrow F^{2me}$	$K_3^2 \rightarrow 0$	$d_2(K_3^2; K_2^2, (K_2 + K_3)^2) + d_2(K_3^2; K_4^2, (K_3 + K_4)^2)$
$F^{3m} \rightarrow F^{2mh}$	$K_2^2 \rightarrow 0$	$\frac{1}{2}d_1(K_2^2) + d_2(K_2^2; K_3^2, (K_2 + K_3)^2)$
$F^{2me} \rightarrow F^{1m}$	$K_2^2 \rightarrow 0$	$d_1(K_2^2)$
$F^{2mh} \rightarrow F^{1m}$	$K_3^2 \rightarrow 0$	$\frac{1}{2}d_1(K_3^2) + d_2(K_3^2; K_4^2, (K_3 + K_4)^2)$
$F^{1m} \rightarrow F^{0m}$	$K_4^2 \rightarrow 0$	$d_1(K_4^2)$

**Table 5:** The discontinuity functions for all scalar box integrals encountered in computations in massless gauge theories. (See fig. 14.)

## 7. Conclusions

In this paper we have provided a general proof and discussion of factorization in massless amplitudes. Infrared divergences associated with massless theories significantly complicate matters as they induce contributions which are not interpreted directly in terms of a naive sum of products of amplitudes with a tree propagator. The loop integrals themselves may contain kinematic poles which cannot be interpreted in any simple way in terms of tree propagators. Furthermore, if the amplitudes contain logarithms in the kinematic variable in which the factorization is being performed, new infrared divergences develop.

Nevertheless, we provided a proof that factorization of massless one-loop gauge theory amplitudes are described by a set of universal functions linked to the known [19,20,21] infrared divergences. In massless (or high-energy) QCD these singularities have been tabulated in previous papers [19,20,21]. The proof presented here was based on general properties of gauge theory amplitudes and not on a specific diagrammatic analysis. In particular, we made use of the reduction of any one-loop amplitude in terms of a basis of scalar box, triangle and bubble functions [36,37,39,38,40,23]. By identifying all possible sources of poles from the loop integrals, a proof was presented which links the coefficients of all such kinematic poles to the known infrared divergences appearing in the amplitudes. The non-factorization of amplitudes is described by a limited set of discontinuity and box integral functions, which were given explicitly. The non-trivial aspect of our proof is that all finite (in  $\epsilon$ ) contributions to non-factorization are fixed in this way.

In particular, we proved the conjecture in ref. [10] that the collinear splitting functions (or amplitudes) determined from one-loop four- [5] and five-point [1,3] amplitudes are universal functions for an arbitrary number of external legs. We also presented a procedure for directly obtaining the splitting functions by calculating only two- and three-point diagrams. Although these diagrams are gauge dependent, after combining these diagrams with discontinuity functions whose coefficients

are fixed by the infrared divergences, the gauge invariant splitting functions are obtained. An explicit sample calculation of the  $g \rightarrow gg$  splitting function in two different gauges was provided. We also calculated the contributions of massive fermions and scalars to these loop splitting functions.

We have also shown how amplitudes factorize on multi-particle poles. Although there are contributions which cannot be interpreted in terms of simple factorization, these are given by a small number of functions whose coefficients are again fixed by infrared divergences. For calculations of six- and higher-point amplitudes multi-particle factorization provides a powerful constraint on the form of the amplitude. An explicit six-point example of the constraints imposed by multi-particle factorization was given.

We have also outlined a procedure for obtaining the splitting functions to higher order in  $\epsilon$ . The higher order terms would be useful for performing phase space integrals at next-to-next-to-leading order using the formalism of ref. [20].

Although we have not explicitly discussed factorization as the momenta of external legs become soft, the same type of analysis performed here may be extended to that case. By a general argument presented in section 5.2, any kinematic poles in the reduction coefficients are proportional to the discontinuity functions.

A spin-off from our analysis is an efficient method for generating dimensionally regularized infrared divergent box integral functions from the known finite massive box integrals. Indeed all box integral functions contained in refs. [23] may be obtained by taking the appropriate massless limits of the massive integrals after subtracting off an appropriate set of discontinuity functions determined by a recursion relation between box and triangle functions. To extend this result to two-loops one would need a way of determining the discontinuities.

The results presented here prove that universal factorization properties hold for any gauge theory one-loop amplitude with an arbitrary number of external legs. We expect factorization to continue to be a powerful tool in the calculation of gauge theory amplitudes.

We thank L. Dixon, D.C. Dunbar, D.A. Kosower and A.G. Morgan for helpful discussions and suggestions. Research supported in part by the US Department of Energy under grant DE-FG03-91ER40662, in part by the National Science Foundation under grant PHY 9218990, and in part by the Alfred P. Sloan Foundation under grant BR-3222.

## Appendix I. Reduction of One-Loop Integrals

In this appendix we review and slightly modify the reduction procedure [36,37,39,38,40,23] that rewrites  $n$ -point integrals in terms of lower-point ones for use in constructing our proof in section 5. This procedure allows any Feynman diagram to be expressed as a linear combination of  $m \leq 4$ -point integrals. The reduction procedure for tensor integrals is a bit different than for scalar integrals so we discuss these cases separately.

### I.1 Tensor Integrals

First we review the reduction of Feynman integrals with a loop momentum dependent numer-

ator and with five or more external legs. Following this, the analogous decomposition of tensor box, triangle, and bubbles is presented.

Consider then the reduction of any tensor integral function with more than four external legs ( $n > 4$ ). Denote by  $I_n[l^{\alpha_1} \dots l^{\alpha_j}]$  the tensor  $n$ -point integral with  $j$  powers of loop momenta in the numerator of the integrand:

$$I_n[l^{\alpha_1} \dots l^{\alpha_j}] \equiv i(-1)^{n+1} (4\pi)^{2-\epsilon} \int \frac{d^{4-2\epsilon} l}{(2\pi)^{4-2\epsilon}} \frac{l^{\alpha_1} \dots l^{\alpha_j}}{(l^2 - m^2)((l - p_1)^2 - m^2) \dots ((l - p_{n-1})^2 - m^2)}, \quad (\text{I.1})$$

where the momentum routing is taken to be  $p_i = \sum_{j=1}^i K_j$ , and the  $K_j$  are adjacent sums of the external momenta of the  $n$ -point amplitude. In gauge theory, in a Feynman-like gauge, the maximum number of powers of loop momentum in the numerator is  $n$  for an  $n$ -point function so  $j \leq n$ . Although we are interested in amplitudes with vanishing internal masses, we have inserted a uniform mass  $m$  in all internal propagators in order to display the difference in the corresponding reduction coefficients. We will show that the pole structure is independent of the mass, a fact we use in section 5 to explain why the poles in the massless reduction coefficients are proportional to discontinuity functions.

The integrals in eq. (I.1) may be reduced by projecting the first component  $\alpha_1$  of the tensor onto a basis of four independent momenta; a simple choice of basis are the four vectors  $p_1, p_2, p_3, p_4$ . The final results for the reduction of the amplitudes are independent of any particular choice of basis. Projecting the loop integral onto the four vectors yields

$$I_n[l^{\alpha_1} l^{\alpha_2} \dots l^{\alpha_j}] = p_1^{\alpha_1} A_1 + p_2^{\alpha_1} A_2 + p_3^{\alpha_1} A_3 + p_4^{\alpha_1} A_4, \quad (\text{I.2})$$

where we have suppressed the indices  $\alpha_2 \dots \alpha_j$  on the right-hand side of eq. (I.2) in  $A_j$ . The functions  $A_i$  are found by first contracting eq. (I.2) with the momenta  $p_i$ , generating the four linearly independent equations,

$$2I_n[l \cdot p_i l^{\alpha_2} \dots l^{\alpha_j}] = \sum_{k=1}^4 t_{ik} A_k, \quad (i = 1, 2, 3, 4), \quad (\text{I.3})$$

where

$$t_{ik} \equiv 2p_i \cdot p_k. \quad (\text{I.4})$$

Since the products  $l \cdot p_i$  within the  $n$ -point integral on the left-hand side of eq. (I.3) may be expressed as

$$2l \cdot p_i = -[(l - p_i)^2 - m^2] + [l^2 - m^2] + p_i^2, \quad (\text{I.5})$$

one can eliminate one of the Feynman denominators with each of the first two terms in eq. (I.5), which gives the integrand for an  $(n - 1)$ -point integral. The third term in eq. (I.5) is independent of the loop momenta and gives an  $n$ -point integral with only  $j - 1$  powers of loop momentum in the integrand.

Thus by solving the linear equations (I.3) for the  $A_i$ , we may express the  $n$ -point integral with  $j$  powers of loop momentum as a linear combination of  $n$ - and  $(n - 1)$ -point integrals with  $j - 1$  powers of loop momentum. By inverting  $t$  we have

$$\begin{aligned} A_i &= \sum_{k=1}^4 \frac{[t]_{ki}}{\Delta} I_n[2l \cdot p_k l^{\alpha_2} \dots l^{\alpha_j}] \\ &= \sum_{k=1}^4 \frac{[t]_{ki}}{\Delta} \left( I_{n-1}^{(k+1)}[l^{\alpha_2} l^{\alpha_3} \dots l^{\alpha_j}] - I_{n-1}^{(1)}[l^{\alpha_2} l^{\alpha_3} \dots l^{\alpha_j}] + p_k^2 I_n[l^{\alpha_2} l^{\alpha_3} \dots l^{\alpha_j}] \right), \end{aligned} \quad (\text{I.6})$$

where the elements  $[t]_{ki}$  in (I.6) are the cofactors of  $t$ . The denominator  $\Delta$  is the Gram determinant of the basis of four vectors,

$$\Delta = \det(t_{ij}). \quad (\text{I.7})$$

(Note the relative signs, between  $I_n$  and  $I_{n-1}$ , in the definition of the integral functions (I.1).)

For dimensionally regularized expressions there is a technicality which must be addressed. Since the expansion on the right-hand side of eq. (I.6) is in terms of a basis of four-dimensional external momenta while the loop momentum on the left-hand side are  $(4 - 2\epsilon)$ -dimensional, one might worry that this could lead to an error. Consider, for example, an  $n$ -point integral with two powers of loop momentum in the numerator. The full  $(4 - 2\epsilon)$  expansion is

$$I_n[l^\alpha l^\beta] = \sum_{i,j=1}^4 p_i^\alpha p_j^\beta A_{ij} + \delta_{[-2\epsilon]}^{\alpha\beta} A_0, \quad (\text{I.8})$$

where  $\delta_{[-2\epsilon]}^{\alpha\beta}$  is a metric which is non-zero only in the  $[-2\epsilon]$ -dimensions. By contracting  $\delta_{[-2\epsilon]}^{\alpha\beta}$  into eq. (I.8) we obtain

$$I_n[-l_\epsilon^2] = -2\epsilon A_0, \quad (\text{I.9})$$

where  $-l_\epsilon^2$  is the  $[-2\epsilon]$  component of  $l^2$ . After Feynman parametrizing the loop integral (I.9) and following the discussion in refs. [9], we break up the momentum integral as

$$\int \frac{d^{4-2\epsilon}l}{(2\pi)^{4-2\epsilon}} = \int \frac{d^4l_4 d^{-2\epsilon}l_\epsilon}{(2\pi)^{4-2\epsilon}} = -\epsilon \frac{(4\pi)^\epsilon}{\Gamma(1-\epsilon)} \int \frac{d^4l_4}{(2\pi)^4} \int_0^\infty dl_\epsilon^2 (l_\epsilon^2)^{-1-\epsilon}. \quad (\text{I.10})$$

Performing the integrals one finds

$$I_n[l_\epsilon^2] = -\epsilon I_n^{D=6-2\epsilon}[1], \quad (\text{I.11})$$

where  $I_n^{D=6-2\epsilon}[1]$  is the  $n$ -point scalar integral in  $D = 6 - 2\epsilon$  dimensions (given in appendix IV.4). Note that  $I_n^{D=6-2\epsilon}$  is completely finite for  $n > 3$ , since there are no infrared or ultraviolet divergences in six dimensions for  $n > 3$ . Thus  $\delta_{[-2\epsilon]}^{\alpha\beta} A_0$  in eq. (I.8) is of  $\mathcal{O}(\epsilon)$  and therefore does not enter into the reduction procedure through  $\mathcal{O}(\epsilon^0)$ . One can easily generalize this argument to show that the difference between a reduction in a four-dimensional basis and a  $(4 - 2\epsilon)$ -dimensional basis is of  $\mathcal{O}(\epsilon)$  as long as no ultra-violet divergences occur in the integrals. In renormalizable gauge theories

(for a Feynman-like gauge) all diagrams with five or more legs are ultra-violet finite, so that the reduction coefficients for  $n \geq 5$  do not depend on  $\epsilon$ . (If one were to keep terms of  $\mathcal{O}(\epsilon)$  or higher, then one would need to keep the higher dimension integrals for  $n \geq 5$ , but these do not possess infrared divergences, discontinuities as an external mass vanishes, or massless poles. Following the discussion in section 5, these do not contribute to non-factorization.)

For  $n \leq 4$  the reduction procedure is similar except that the integral does not contain a complete set of external momenta that spans four dimensions, so we must include the metric tensor. The metric tensor must be taken to be  $4 - 2\epsilon$  dimensional since ultra-violet divergences are encountered: boxes with four powers, triangles with two or more powers of momentum, and bubble integrals are all ultraviolet divergent. The reduction coefficients of such integrals can be expected to contain  $\epsilon$ -dependence. (In the case of supersymmetric theories, one can arrange all  $n \geq 3$  integrals to have at least two powers less of loop momentum in the numerator so that all integrals with  $n \geq 3$  are ultra-violet finite; this means that the reduction coefficients are independent of  $\epsilon$  in supersymmetric theories [11].)

Consider the standard expansion of the tensor integrals for  $n \leq 4$ ,

$$I_n[l^\alpha] = A_{1;i} p_i^\alpha, \quad (\text{I.12a})$$

$$I_n[l^{\alpha_1} l^{\alpha_2}] = A_{2;0} \delta_{[4-2\epsilon]}^{\alpha_1 \alpha_2} + A_{2;i,j} p_i^{\alpha_1} p_j^{\alpha_2}, \quad (\text{I.12b})$$

$$I_n[l^{\alpha_1} l^{\alpha_2} l^{\alpha_3}] = A_{3;i} \left[ \delta_{[4-2\epsilon]}^{\alpha_1 \alpha_2} p_i^{\alpha_3} + \delta_{[4-2\epsilon]}^{\alpha_1 \alpha_3} p_i^{\alpha_2} + \delta_{[4-2\epsilon]}^{\alpha_2 \alpha_3} p_i^{\alpha_1} \right] + A_{3;i,j,k} p_i^{\alpha_1} p_j^{\alpha_2} p_k^{\alpha_3}, \quad (\text{I.12c})$$

$$I_n[l^{\alpha_1} l^{\alpha_2} l^{\alpha_3} l^{\alpha_4}] = A_{4;0} \left[ \delta_{[4-2\epsilon]}^{\alpha_1 \alpha_2} \delta_{[4-2\epsilon]}^{\alpha_3 \alpha_4} + \delta_{[4-2\epsilon]}^{\alpha_1 \alpha_3} \delta_{[4-2\epsilon]}^{\alpha_2 \alpha_4} + \delta_{[4-2\epsilon]}^{\alpha_1 \alpha_4} \delta_{[4-2\epsilon]}^{\alpha_2 \alpha_3} \right] \\ + A_{4;ij} \left[ \delta_{[4-2\epsilon]}^{\alpha_1 \alpha_2} p_i^{\alpha_3} p_j^{\alpha_4} + \text{sym.} \right] + A_{4;i,j,k,l} p_i^{\alpha_1} p_j^{\alpha_2} p_k^{\alpha_3} p_l^{\alpha_4}, \quad (\text{I.12d})$$

where the repeated indices are implicitly summed over and some of the coefficients are related by symmetry. By dotting the momenta  $p_i$  into these equations and contracting various indices one obtains a complete set of equations which may be solved for the coefficients  $A$ . The equations obtained by contracting indices contain explicit  $\epsilon$ -dependence through  $\delta_{[4-2\epsilon]}^{\alpha\beta} \delta_{\alpha\beta}^{[4-2\epsilon]} = 4 - 2\epsilon$ .

We now outline a modified procedure which eliminates explicit  $\epsilon$ -dependence from the equations obtained by contracting indices. Consider the first integral (I.12a); in this case the metric tensor does not appear and the  $A_{1;i}$  may be solved by dotting external momenta into eq. (I.12a); no  $\epsilon$ -dependence enters in these equations.

Next we have the integral (I.12b), which has a  $\delta_{[4-2\epsilon]}^{\alpha_1 \alpha_2}$  in the tensor expansion. To solve for the  $A_{2;0}$  we perform instead the contractions with the tensor  $\delta_{[-2\epsilon]}^{\alpha_1 \alpha_2}$  which is non-zero only for the  $[-2\epsilon]$  dimensions. Performing the contraction of eq. (I.12b) with  $\delta_{[-2\epsilon]}^{\alpha_1 \alpha_2}$  we obtain

$$I_n[l_\epsilon^2] = -\epsilon I_n^{D=6-2\epsilon}[1] = 2\epsilon A_{2;0}, \quad (\text{I.13})$$

so that

$$A_{2;0} = -\frac{1}{2} I_n^{D=6-2\epsilon}[1]. \quad (\text{I.14})$$

The coefficient of  $I_n^{D=6-2\epsilon}[1]$  does not contain  $\epsilon$ -dependence. The remaining equations for  $A_{2;i,j}$  obtained by dotting into external momenta are manifestly free of  $\epsilon$ .

For  $I_n[l^{\alpha_1}l^{\alpha_2}l^{\alpha_3}]$  we may contract eq.(I.12c) with  $2\delta_{[-2\epsilon]}^{\alpha_1\alpha_2}p_m^{\alpha_3}$  to obtain

$$2I_n[l_\epsilon^2 l \cdot p_j] = 2\epsilon \sum_{i=1}^{n-1} A_{3;i} t_{ji}. \quad (\text{I.15})$$

Using the expansion  $2l \cdot p_j = -[(l-p_j)^2 - m^2] + [l^2 - m^2] + p_j^2$  and eq. (I.11) we obtain the expanded form

$$2I_n[l_\epsilon^2 l \cdot p_j] = -\epsilon \left( I_{n-1}^{(j+1),D=6-2\epsilon} - I_{n-1}^{(1),D=6-2\epsilon} + p_j^2 I_n^{D=6-2\epsilon} \right). \quad (\text{I.16})$$

By inverting eq. (I.15) we then have

$$A_{3;i} = -\frac{1}{2} \sum_{j=1}^{n-1} t_{ij}^{-1} \left[ I_{n-1}^{(j+1),D=6-2\epsilon}[1] - I_{n-1}^{(1),D=6-2\epsilon}[1] + p_j^2 I_n^{D=6-2\epsilon}[1] \right]. \quad (\text{I.17})$$

Note again that there is no  $\epsilon$ -dependence in the coefficients of the integrals. Further equations which are obtained by only dotting external momenta into eq. (I.12c) are manifestly independent of  $\epsilon$ .

Finally, consider the case of four powers of loop momentum in the numerator. If we contract eq. (I.12d) with  $\delta_{[-2\epsilon]}^{\alpha_1\alpha_2}\delta_{[-2\epsilon]}^{\alpha_3\alpha_4}$  we obtain

$$I_n[l_\epsilon^4] = -\epsilon(1-\epsilon)I_n^{D=8-2\epsilon} = (4\epsilon^2 - 4\epsilon)A_{4;0}, \quad (\text{I.18})$$

so that

$$A_{4;0} = \frac{1}{4}I_n^{D=8-2\epsilon}. \quad (\text{I.19})$$

Once again all  $\epsilon$ -dependence cancels from the coefficients. The other coefficients may be obtained by continuing the reduction process and are also free of  $\epsilon$ .

Thus, by introducing the  $D = 6 - 2\epsilon$  and  $D = 8 - 2\epsilon$  dimension scalar bubble, triangle and box functions (given in appendix IV.4) we may avoid  $\epsilon$ -dependence in the reduction coefficients; this dependence has been pushed into these integrals. (In the dimensional reduction [28] or FDH [5] schemes there are no other sources of  $\epsilon$  dependence, since the numbers of particle states are the four dimensional ones.) Upon rewriting the higher-dimensional integral functions in terms of  $D = 4 - 2\epsilon$  ones, the conventional reduction (through  $\mathcal{O}(\epsilon^0)$ ) is regained.

As an explicit example of the modified reduction procedure consider the tensor bubble integral in a massless theory

$$\begin{aligned} I_2[l^\mu l^\nu] &= -i(4\pi)^{2-\epsilon} \int \frac{d^{4-2\epsilon}l}{(2\pi)^{4-2\epsilon}} \frac{l^\mu l^\nu}{l^2(l-K)^2} \\ &\equiv B_1 \delta_{[4-2\epsilon]}^{\mu\nu} K^2 + B_2 K^\mu K^\nu. \end{aligned} \quad (\text{I.20})$$

First consider a conventional reduction procedure. By either tracing over the indices with  $\delta_{[4-2\epsilon]}^{\mu\nu}$  or dotting into the  $K^\mu K^\nu$  we obtain the two equations

$$(4-2\epsilon)B_1 + B_2 = 0, \quad (B_1 + B_2) = \frac{1}{4}I_2[1], \quad (\text{I.21})$$

where we used  $2K \cdot l = -(l - K)^2 + l^2 + K^2$  and also dropped the tadpole diagrams, which vanish in dimensional regularization. (For higher-point functions it is more convenient to dot only one momentum at a time into the expansion for the integrals, followed by iterating the equations for each power of loop momentum.) Solving the two equations we have

$$B_1 = -\frac{1}{4} \frac{1}{3 - 2\epsilon} I_2[1], \quad B_2 = \frac{1}{2} \frac{2 - \epsilon}{3 - 2\epsilon} I_2[1], \quad (\text{I.22})$$

which contain explicit  $\epsilon$ -dependence in the coefficient of the scalar bubble integral; it is this  $\epsilon$ -dependence which we wish to avoid by using the modified procedure.

Now consider the modified procedure, where we extend our basis of integral functions to include the six-dimensional bubble. We obtain the first equation by tracing over the  $[-2\epsilon]$  dimensions in eq. (I.20) to yield

$$\begin{aligned} I_2[l_\epsilon^2] &= 2\epsilon B_1 K^2 \\ &= -\epsilon I_2^{D=6-2\epsilon}[1], \end{aligned} \quad (\text{I.23})$$

which we may use to solve for  $B_1$ . The second equation is obtained by dotting  $K^\mu K^\nu$  into eq. (I.20)

$$B_1 + B_2 = \frac{1}{4} I_2[1], \quad (\text{I.24})$$

so that

$$B_1 = -\frac{1}{2K^2} I_2^{D=6-2\epsilon}, \quad B_2 = \frac{1}{4} I_2[1] + \frac{1}{2K^2} I_2^{D=6-2\epsilon}. \quad (\text{I.25})$$

Note that there is no  $\epsilon$ -dependence in the coefficients of the integral functions in eq. (I.25). It is easy to verify that this solution is identical to the one in eq. (I.22) after using eq. (IV.20) to express the  $D = 6 - 2\epsilon$  integral functions in terms of  $D = 4 - 2\epsilon$  ones.

## I.2 Scalar Integrals

Consider now  $n$ -point scalar integrals with  $n > 5$ . Denote by  $I_n[1]$  the scalar  $n$ -gon integral with no powers of loop momenta in the numerator of the integrand:

$$I_n[1] \equiv i(-1)^{n+1} (4\pi)^{2-\epsilon} \int \frac{d^{4-2\epsilon} l}{(2\pi)^{4-2\epsilon}} \frac{1}{(l^2 - m^2)((l - p_1)^2 - m^2) \cdots ((l - p_{n-1})^2 - m^2)}. \quad (\text{I.26})$$

A convenient method for reducing the integral in eq. (I.26) is given in ref. [38]. This method is based on the observation that for four-dimensional momenta defined by  $p_i = \sum_{j=1}^i K_j$ , and for  $n > 5$  point integrals a solution to

$$\sum_{i=1}^6 b_i p_i^\alpha = 0, \quad \sum_{i=1}^6 b_i = 0, \quad (\text{I.27})$$

can be found for some constants  $b_i$ . At least six  $b_i$  are required for a non-trivial solution since five or more vectors are linearly dependent in four-dimensions and the second equation provides an additional constraint. For  $n = 5$  this solution breaks down because there are only four independent

momenta present within the integral; another technique [39,40,23] may be used to reduce scalar pentagons whose results we quote below.

The reduction for  $n > 5$  proceeds by first multiplying the integrand of eq. (I.26) by unity in the form,

$$1 = \frac{\sum_i b_i (p_i^2 - m^2)}{\sum_i b_i (p_i^2 - m^2)}, \quad (\text{I.28})$$

and using the properties of  $b_i$  (i.e.,  $\sum_i b_i l^2 = 0$  and  $\sum_i b_i l \cdot p_i = 0$ ) so that we may express the numerator in eq. (I.28) as

$$\sum_{i=1}^6 b_i (p_i^2 - m^2) = \sum_{i=1}^6 b_i ((l - p_i)^2 - m^2), \quad (\text{I.29})$$

which corresponds to a sum over factors in the denominator of the integrand in eq. (I.26). The mass dependence in the denominator of eq. (I.28) also drops out via  $\sum_{i=1}^6 b_i m^2 = 0$ , and the original integral in eq. (I.26) may then be expanded as,

$$\begin{aligned} I_n[1] &= \frac{1}{\sum_{j=1}^6 b_j p_j^2} \sum_{i=1}^6 b_i I_n[(l - p_i)^2 - m^2] \\ &= -\frac{1}{\sum_{j=1}^6 b_j p_j^2} \sum_{i=1}^6 b_i I_{n-1}^{(i+1)}[1], \end{aligned} \quad (\text{I.30})$$

where  $I_{n-1}^{(i)}$  is the  $(n-1)$ -point integral obtained from the  $n$ -point integral by removing the propagator in eq. (I.26) between legs  $i-1$  and  $i$ .

The solution of eqs. (I.27) are ratios of kinematic determinants, given in detail by Melrose [38] The result in solving for the  $b_i$  is that the coefficients in front of the  $I_{n-1}^{(i+1)}$  in eq. (I.30) are inversely proportional to

$$\det \left[ -\frac{1}{2} (p_{i-1} - p_{j-1})^2 \right]. \quad (\text{I.31})$$

Any poles in the scalar integral reduction coefficients (for  $n \geq 6$ ), for the case of a uniform or zero internal mass, must come from this determinant. Since the mass dependence  $m$  in the integral reduction coefficients drops out for the case of a uniform mass around the loop, the poles for  $m = 0$  or  $m \neq 0$  are the same.

This leaves us with the special case of  $n = 5$ , that is, the reduction of scalar pentagon integrals down to boxes. For this case, we quote the results of ref. [40]. The scalar pentagon with a uniform internal mass and external momenta  $K_i$  may be expressed as

$$I_5 = \frac{1}{2} \sum_{i=1}^5 c_i I_4^{(i)} + \epsilon c_0 I_5^{D=6-2\epsilon}, \quad (\text{I.32})$$

where

$$c_i = \sum_{j=1}^5 S_{ij}^{-1}, \quad c_0 = \sum_{i=1}^5 c_i, \quad S_{ij} = m^2 - \frac{1}{2} (p_{i-1} - p_{j-1})^2. \quad (\text{I.33})$$



In summary, by iterating the above tensor and scalar reduction procedures from  $n$ - to  $(n - 1)$ -point integrals any  $D = 4 - 2\epsilon$  one-loop amplitude may be expressed as a linear combination of scalar bubble, triangle, and box integral functions. By using a slightly modified Passarino-Veltman reduction of tensor integrals we avoid all  $\epsilon$ -dependence in the reduction coefficients at the cost of introducing higher-dimensional scalar integrals. The explicit forms of scalar functions which may appear in massless gauge theories is summarized in appendix IV.

## Appendix II. Kinematic Poles in Reduction Coefficients

In this appendix we find the potential kinematic poles in a particular channel within the integral reduction coefficients, reviewed in the previous appendix. We will systematically step through and discuss the various kinematic denominators of the coefficients to exhibit their structure. Furthermore, we find that one can side-step the poles in a given channel for the reduction of integrals down to  $n = 5$  and  $n = 6$  for tensor and scalar integrals, respectively. We also track the difference in the kinematic denominators when there is a uniform internal mass in the loop and when there is no mass, which is used in section 5 to understand why these poles are proportional to discontinuity functions.

### II.1 Poles from $n \geq 6$ integral reductions

The coefficients which may appear, in each step of the reduction of integrals with six or more external legs, are proportional to the inverses of the two kinematic determinants given in eqs. (I.7) and (I.31),

$$\begin{aligned} \text{(a)} \quad & \det[2p_{\sigma_i} \cdot p_{\sigma_j}], & (i, j = 1, \dots, 4), \\ \text{(b)} \quad & \det[-\frac{1}{2}(p_{\sigma_i} - p_{\sigma_j})^2], & (i, j = 1, \dots, 6), \end{aligned} \tag{II.1}$$

where the  $p_{\sigma_j}$  (with  $j = 1 \dots n - 1$ ) are any of the  $p_i = \sum_j K_j$ . The  $K_j$  are external momenta of the integral function being reduced and may be on- or off-shell. The final result for the amplitudes is independent of any particular choice of the bases  $\{p_{\sigma_j}\}$  at each step of the procedure. (This clearly holds for tensor reductions [36,39] and has been explicitly shown by Melrose [38] for the case of scalar reductions.) The first determinant (a) is the Gram determinant arising from tensor reductions, while the second (b) is a modified Cayley determinant coming from the reduction of scalar integrals.

Whenever either of these determinants has zeros the reduction coefficients can have poles. The Gram determinant will vanish whenever the momentum basis of the reduction collapses, which may happen if two (even non-adjacent) massless external momenta are collinear or one external momentum is soft. Note that as a multi-particle kinematic variable vanishes, the two determinants considered as general analytic functions will not vanish (except for special kinematics, such as when all kinematic variables are time-like); thus we only need consider collinear (and soft) poles.

In any channel where the momenta of given pair of external legs become collinear one can avoid zeros in the determinants (a) and (b) by a judicious choice of the momentum basis. For example,

by not including either  $p_1$  or  $p_2$  in the basis, as the momenta of legs 1 and 2 become collinear the Gram determinant (a) does not vanish. (For  $n \geq 6$  there are always at least five momenta from which to choose the four needed in the Gram determinant.) In this way we may avoid collinear poles in any given channel coming from the tensor reduction coefficients for  $n \geq 6$ . The same type of reasoning allows one to avoid zeros in the second determinant (b) for  $n > 6$ . For the case of  $n = 6$  one may explicitly check that there are zeros. Thus by making use of arbitrariness in the momentum basis choice of the reduction one can avoid the poles in the coefficients in any channel of the  $n$  goes to  $n - 1$  reduction, down to scalar hexagons ( $n = 6$ ). The poles in the scalar hexagon reduction coefficient do not, however, depend on the uniform internal mass.

In another channel one would choose a different momentum basis to again avoid poles in  $n > 6$  reduction coefficients. The consistency of this procedure follows from the fact that all final results for amplitudes are independent of the choice of basis in each step; a change of momentum basis only shifts the poles to different steps of the reduction. Our choice is to always push the collinear pole in any given channel to the scalar hexagon and the pentagon reduction, discussed below.

## II.2 Poles from $n \leq 5$ integral reductions

Now consider the potential kinematic poles that arise from the reduction of  $n \leq 5$  point integrals. As discussed in the previous appendix, the only denominators which may appear are

$$\begin{aligned} \text{(a)} \quad \Delta &= \det[2p_i \cdot p_j] = \det[2K_i \cdot K_j], & (1 \leq i, j \leq n - 1 \leq 4), \\ \text{(b)} \quad \det S &= \det \left[ m^2 - \frac{1}{2}(p_{i-1} - p_{j-1})^2 \right], & (i, j = 1, \dots, 5), \end{aligned} \quad (\text{II.2})$$

where  $m$  is a uniform mass in the loop. The first one comes from tensor reductions with  $n \leq 5$  and the second from reducing scalar pentagons as given in eq. (I.32). There are no multi-particle zeros in either determinant for  $n > 2$ . For  $n = 2$  the multi-particle pole appearing in the reduction coefficient of the tensor bubble (I.25) multiplies  $I_2^{D=6-2\epsilon}$ , given in eq. (IV.20), which then cancels the pole. One cannot avoid collinear poles for  $n \leq 5$  since there is only one basis choice for the reduction of these integrals; the poles which have been side-stepped above for  $n \geq 6$  appear here. For example, as  $s_{12} \rightarrow 0$  the diagram depicted in fig. 11, with on-shell legs  $k_1$  and  $k_2$ , is the only type of pentagon which has a pole in this channel.

The Gram determinant (a), which has no dependence on the uniform internal mass, contains zeros whenever any pair of on-shell momenta  $K_i = k_i$  become collinear. (Recall that lower case momenta denote on-shell external momenta of the amplitude.)

For the case of  $m = 0$ , it is straightforward to investigate zeros of the second determinant (b) in multi-particle and collinear channels. As a multi-particle kinematic variable  $t_i^{[r]}$  ( $r > 2$ ) vanishes  $\det S$  will not vanish (except for special kinematic configurations). There will however be zeros in  $\det S$  for collinear massless momenta. For example, the kinematic configuration in fig. 11 gives

$$\det S = -\frac{1}{16} s_{12} \left( s_{23} s_{34} s_{45} s_{51} - s_{23} s_{12} s_{51} K_4^2 + s_{51} K_3^2 K_5^2 s_{23} - s_{34} K_5^2 s_{23}^2 - K_3^2 s_{45} s_{51}^2 \right), \quad (\text{II.3})$$

which clearly vanishes in the limit  $s_{12} \rightarrow 0$ . Thus, poles of the form  $1/s_{i,i+1}$  may develop in the reduction of scalar pentagons to scalar boxes.

For the case of  $m \neq 0$ , the second determinant (b) contains explicit dependence on the uniform internal mass. However, this dependence is relatively simple since

$$\det S \Big|_{m \neq 0} = \det S \Big|_{m=0} + \frac{m}{16} \Delta. \quad (\text{II.4})$$

The Gram determinant has zeros whenever  $\det S|_{m=0}$  has one, so that  $\det S|_{m \neq 0}$  will have the same zeros as  $\det S|_{m=0}$ .

In summary, in any given multi-particle or collinear channel the integral reduction may be performed so that there are no poles in the coefficients for  $n > 6$ . For  $n \leq 6$  poles may appear as momenta become collinear (or soft). However, one finds the same apparent poles in the reduction of loop integrals containing a uniform internal mass as for the massless case.

### Appendix III. Higher Dimension Integrals: Special Cases

In this appendix we show that the two special cases, the higher dimension integrals  $I_2^{D=6-2\epsilon}$  and  $I_3^{1m, D=6-2\epsilon}$  in eq. (5.11), do not contribute as discontinuity functions. Both are proportional (with  $\epsilon$  dependent coefficients) to the  $D = 4 - 2\epsilon$  scalar bubble in eq. (IV.2), which becomes a discontinuity function as the single external mass vanishes. The potential appearance of these integrals as discontinuity functions might introduce contributions to the splitting and factorization functions not linked to the singularities in  $\epsilon$ . In this appendix we show that such potential contributions do not occur.

For both the bubble  $I_2^{D=6-2\epsilon}(K^2)$  and triangle  $I_3^{1m, D=6-2\epsilon}(K^2)$  we will examine the appearance of poles in the  $K^2$  channel. Poles may in principle come from either tree propagators, as discussed in section 5.1 or from reduction coefficients, as in section 5.2. (These two higher-dimensional integral functions themselves do not have poles.)

First consider the appearance of  $I_2^{D=6-2\epsilon}$ . As discussed in appendix I, the Passarino-Veltman reduction takes an  $n$ -point integral function with  $m$  powers of loop momentum and reduces it to a combination of  $n$  and  $n - 1$  point integral functions with  $m - 1$  powers of loop momentum. Thus the only way to obtain a tensor bubble (two-point) integral function with two powers of loop momentum, which generate the  $D = 6 - 2\epsilon$  scalar bubbles via equations (I.20) and (I.25), is to start with an  $m$ -point integral with  $m$  powers of loop momentum in the numerator. Thus, to obtain  $D = 6 - 2\epsilon$  bubble functions we must consider (maximal) tensor integral functions of the form

$$I_m[l^{\alpha_1} \dots l^{\alpha_m}] \equiv i(-1)^{n+1}(4\pi)^{2-\epsilon} \int \frac{d^{4-2\epsilon}l}{(2\pi)^{4-2\epsilon}} \frac{l^{\alpha_1} \dots l^{\alpha_m}}{l^2 (l - K_1)^2 \dots (l - K_m)^2}, \quad (\text{III.1})$$

In ordinary or background field Feynman gauge this maximum occurs for diagrams where all legs attached to the loop are gauge boson legs [11]; diagrams where fermion lines are entering or exiting

the loop will have one less power of loop momentum. Thus we need consider loops with only gluons attached.

First consider the case where the kinematic pole arises from a reduction coefficient. As discussed in appendix II, no multi-particle poles arise from reduction coefficients. For the case of two-particle (collinear) poles one can side-step the poles from tensor integrals down to pentagons, as discussed in appendix II.1. Furthermore, for the pentagon and below, using the formulas of appendix I, it is straightforward to check that the coefficients of the  $D = 6 - 2\epsilon$  bubbles contain at most a single pole in any given channel. Since  $I_2^{D=6-2\epsilon}[1](K^2)$  is proportional to  $(K^2)^{1-\epsilon}$  the pole is spurious since it is canceled. Alternatively, one may investigate the  $m$ -point loop integrals with  $m$  powers of loop momentum directly; this type of analysis has already been discussed in ref. [13,15] with the result that they do not contribute a pole to the amplitude.

Now consider the bubble function  $I_2^{D=6-2\epsilon}$  from diagrams with a tree propagator as on the right-hand-side of fig. 5. The bubble functions can arise either directly from diagrams with two-point loops or from the integral reduction of higher-point loop diagrams. The diagrams with a bubble loop are part of the ‘factorizing’ contribution and therefore do not concern us in this appendix. For the bubble functions that arise from higher-point diagrams we show below that all integrals with a maximum number of powers of loop momentum suppress the pole from the intermediate leg, since they are proportional to either

$$K^2 \delta_{[4-2\epsilon]}^{\alpha_1 \alpha_i} \quad \text{or} \quad K^{\alpha_1}, \quad (\text{III.2})$$

where the index  $\alpha_1$  dots into the gluon (or gauge boson) line of the intermediate factorized leg and  $K_1 = K$  in eq. (III.1). The integrals cannot produce any further poles in external mass  $K^2$ , as can be seen from the fact that such poles do not exist in the reduction coefficients, discussed in appendix II, or in the basis of integral functions, discussed in appendix IV. (The  $D = 4 - 2\epsilon$  single mass triangles are an exception, but such integrals with more than four-point kinematics do not occur in the reduction of diagrams with tree poles that we are considering.) The first type of term is clearly subdominant in the factorization since the factor of  $K^2$  cancels the pole from the tree propagator. The second type of term is also subdominant because the gluon contracts against a tree amplitude which makes up a conserved current; the longitudinal term vanishes sufficiently fast to be irrelevant.

First we contract eq. (III.1) with the external momentum  $K_1^{\alpha_1}$  and rewrite the scalar product as  $2l \cdot K_1 = -(l - K_1)^2 + l^2 + K_1^2$ . This produces three new integrals,

$$2I_m[l \cdot K_1 l^{\alpha_2} \dots l^{\alpha_m}] = I_{m-1}^{(2)}[l^{\alpha_2} \dots l^{\alpha_m}] - I_{m-1}^{(1)}[l^{\alpha_2} \dots l^{\alpha_m}] + K_1^2 I_m[l^{\alpha_2} \dots l^{\alpha_m}], \quad (\text{III.3})$$

where  $I_{m-1}^{(j)}$  is the loop integral with  $m-1$  legs obtained from (III.1) by removing the  $j$ th propagator.

The first two integrals are functions of  $K_1 + K_2$  and  $K_1 + K_m$  and will never reduce further into a bubble integral with momentum  $K_1^\alpha$  flowing through. The third integral does not possess a  $K_1^2$  pole within the integral function and is then suppressed by a factor of  $K_1^2$  in front. Thus in the factorizing limit there is no unsuppressed contribution.

Dotting the integral (III.1) into  $K_1^\alpha$  leads only to potential discontinuities suppressed by  $K_1^2$ ; this necessarily means that the integral (III.1) must be proportional to either of the two tensors in eq. (III.2), which as discussed above are suppressed in the factorization limit.

The single-external-mass triangle  $I_3^{1m, D=6-2\epsilon}$  (IV.21) also requires special care as it is discontinuous in the limit that the external mass vanishes. The argument of these integrals are the  $s_{i, i+1}$  where  $i$  and  $i + 1$  label the momenta of two massless legs of the triangle. Such triangles are only discontinuous for the collinear or soft limits of  $k_i$  and  $k_{i+1}$ . In the integral reduction, this triangle function can appear from two places. The first is from the factorizing diagrams displayed in fig. 2. The integrals from these diagrams are directly taken into account in our analysis since we calculate them explicitly; indeed, a combination of  $D = 4 - 2\epsilon$  and  $D = 6 - 2\epsilon$  integrals from these diagrams is what makes  $\text{Split}^{\text{fact}}$  non-zero in eq. (3.7).

The second place  $I_3^{1m, D=6-2\epsilon}$  may arise is in the reduction of integrals of the form in fig. 10, which is given for the  $s_{12}$  channel (all remaining  $s_{i, i+1}$  channels are similar); in this figure  $I_3^{1m, D=6-2\epsilon}$  would arise in the reduction term where all loop propagators between  $k_3$  and  $k_n$  (following the clockwise ordering) are removed; the single external mass in this case is  $s_{12}$ . As discussed in appendix II, down to pentagon integrals we can avoid poles from tensor integrals in any given channel by choosing an appropriate momentum basis in which to perform the reduction. For the pentagon to box, and box to triangle reductions it is straightforward to verify, using the formulas of appendix I, that the coefficient of  $I_3^{1m, D=6-2\epsilon}(s_{12})$  does not have a pole as  $s_{12} \rightarrow 0$ . Thus  $I_3^{1m, D=6-2\epsilon}(s_{12})$  does not contribute to the non-factorizing parts of the splitting and factorization functions.

## Appendix IV. The Basis of Integral Functions

In this appendix we collect the integral functions useful for the discussions in the text; these integral functions were obtained from ref. [40,23]. The  $n$ -point scalar one-loop integral in  $4 - 2\epsilon$  dimensions is

$$I_n = (-1)^{n+1} i (4\pi)^{2-\epsilon} \int \frac{d^{4-2\epsilon}p}{(2\pi)^{4-2\epsilon}} \frac{1}{p^2(p - K_1)^2(p - K_1 - K_2)^2 \cdots (p - K_1 - K_2 - \cdots - K_{n-1})^2}, \quad (\text{IV.1})$$

where  $K_i, i = 1, \dots, n$  are the external momenta, which may be either on- or off-shell. As discussed in appendix I any gauge theory one-loop amplitude can be reduced to a linear combination of (a)  $D = 4 - 2\epsilon$  scalar box, triangle and bubble integrals, (b)  $D = 6 - 2\epsilon$  scalar triangle and bubble integrals and (c)  $D = 8 - 2\epsilon$  box integrals. The higher dimension scalar integrals are defined by replacing the  $4 - 2\epsilon$  in eq. (IV.1) with the appropriate dimension  $D$ . Following the conventions of ref. [23] integrals without a dimension label are taken to be in  $D = 4 - 2\epsilon$ . We first present the  $D = 4 - 2\epsilon$  integrals and subsequently give the higher dimension ones.

### IV.1 Bubble functions

The  $D = 4 - 2\epsilon$  two-point integral function is

$$I_2(K^2) = \frac{r_\Gamma}{\epsilon(1 - 2\epsilon)} (-K^2)^{-\epsilon}, \quad (\text{IV.2})$$

where

$$r_\Gamma = \frac{\Gamma(1+\epsilon)\Gamma^2(1-\epsilon)}{\Gamma(1-2\epsilon)}. \quad (\text{IV.3})$$

## IV.2 Triangle functions

In fig. 9 the three types of triangle integral functions that may appear in massless gauge theories are given. The three  $D = 4 - 2\epsilon$  scalar triangle functions are

$$I_3^{3\text{m}}(K_1^2, K_2^2, K_3^2) = \frac{i}{\sqrt{\Delta_3}} \sum_{j=1}^3 \left[ \text{Li}_2 \left( - \left( \frac{1+i\delta_j}{1-i\delta_j} \right) \right) - \text{Li}_2 \left( - \left( \frac{1-i\delta_j}{1+i\delta_j} \right) \right) \right], \quad (\text{IV.4a})$$

$$I_3^{2\text{m}}(K_1^2, K_2^2) = \frac{r_\Gamma}{\epsilon^2} \frac{(-K_1^2)^{-\epsilon} - (-K_2^2)^{-\epsilon}}{(-K_1^2) - (-K_2^2)}, \quad (\text{IV.4b})$$

$$I_3^{1\text{m}}(K_1^2) = \frac{r_\Gamma}{\epsilon^2} (-K_1^2)^{-1-\epsilon}, \quad (\text{IV.4c})$$

where

$$\delta_1 = \frac{K_1^2 - K_2^2 - K_3^2}{\sqrt{\Delta_3}}, \quad \delta_2 = \frac{-K_1^2 + K_2^2 - K_3^2}{\sqrt{\Delta_3}}, \quad \delta_3 = \frac{-K_1^2 - K_2^2 + K_3^2}{\sqrt{\Delta_3}}, \quad (\text{IV.5})$$

and

$$\Delta_3 \equiv -(K_1^2)^2 - (K_2^2)^2 - (K_3^2)^2 + 2K_1^2 K_2^2 + 2K_2^2 K_3^2 + 2K_3^2 K_1^2. \quad (\text{IV.6})$$

For our purposes it is a bit more convenient to deal with integral functions where the denominators have been scaled out so we define

$$I_3^{3\text{m}}(K_1^2, K_2^2, K_3^2) = i \frac{r_\Gamma}{\sqrt{\Delta_3}} T_3^{3\text{m}}(K_1^2, K_2^2, K_3^2), \quad (\text{IV.7a})$$

$$I_3^{2\text{m}}(K_1^2, K_2^2) = \frac{r_\Gamma}{K_1^2 - K_2^2} T_3^{2\text{m}}(K_1^2, K_2^2), \quad (\text{IV.7b})$$

$$I_3^{1\text{m}}(K_1^2) = -\frac{r_\Gamma}{K_1^2} T_3^{1\text{m}}(K_1^2) \quad (\text{IV.7c}).$$

## IV.3 Box Functions

The scalar box (four-point) functions appearing in computations with massless internal lines have already been extensively discussed in refs. [22,23]. The reader is referred to these papers for further details. It is convenient to define this function as

$$F(K_1, K_2, K_3, K_4) = -\frac{2\sqrt{\det S}}{r_\Gamma} I_4, \quad (\text{IV.8})$$

where the symmetric  $4 \times 4$  matrix  $S$  has components ( $i, j$  are mod 4)

$$S_{ij} = -\frac{1}{2} (K_i + \dots + K_{j-1})^2, \quad i \neq j; \quad S_{ii} = 0. \quad (\text{IV.9})$$

The external momentum arguments  $K_{1\dots 4}$  in equation (IV.8) are sums of external momenta  $k_i$  that are the arguments of the  $n$ -point amplitude. From ref. [23], through  $\mathcal{O}(\epsilon^0)$ , we have (after correcting a sign in the first box function)

$$F^{4m}(K_1, K_2, K_3, K_4) = \frac{1}{2} \left\{ -\text{Li}_2\left(\frac{1}{2}(1 - \lambda_1 + \lambda_2 + \rho)\right) + \text{Li}_2\left(\frac{1}{2}(1 - \lambda_1 + \lambda_2 - \rho)\right) \right. \\ \left. - \text{Li}_2\left(-\frac{1}{2\lambda_1}(1 - \lambda_1 - \lambda_2 - \rho)\right) + \text{Li}_2\left(-\frac{1}{2\lambda_1}(1 - \lambda_1 - \lambda_2 + \rho)\right) \right. \\ \left. - \frac{1}{2} \ln\left(\frac{\lambda_1}{\lambda_2^2}\right) \ln\left(\frac{1 + \lambda_1 - \lambda_2 + \rho}{1 + \lambda_1 - \lambda_2 - \rho}\right) \right\}, \quad (\text{IV.10a})$$

$$F^{3m}(k_1, K_2, K_3, K_4) = -\frac{1}{\epsilon^2} \left[ (-s)^{-\epsilon} + (-t)^{-\epsilon} - (-K_2^2)^{-\epsilon} - (-K_3^2)^{-\epsilon} - (-K_4^2)^{-\epsilon} \right] \\ - \frac{1}{2\epsilon^2} \left( \frac{(-K_2^2)(-K_3^2)}{(-t)} \right)^{-\epsilon} - \frac{1}{2\epsilon^2} \left( \frac{(-K_3^2)(-K_4^2)}{(-s)} \right)^{-\epsilon} \\ + \text{Li}_2\left(1 - \frac{K_2^2}{s}\right) + \text{Li}_2\left(1 - \frac{K_4^2}{t}\right) - \text{Li}_2\left(1 - \frac{K_2^2 K_4^2}{st}\right) + \frac{1}{2} \ln^2\left(\frac{s}{t}\right), \quad (\text{IV.10b})$$

$$F^{2mh}(k_1, k_2, K_3, K_4) = -\frac{1}{\epsilon^2} \left[ (-s)^{-\epsilon} + (-t)^{-\epsilon} - (-K_3^2)^{-\epsilon} - (-K_4^2)^{-\epsilon} \right] - \frac{1}{2\epsilon^2} \left( \frac{(-K_3^2)(-K_4^2)}{(-s)} \right)^{-\epsilon} \\ + \text{Li}_2\left(1 - \frac{K_3^2}{t}\right) + \text{Li}_2\left(1 - \frac{K_4^2}{t}\right) + \frac{1}{2} \ln^2\left(\frac{s}{t}\right), \quad (\text{IV.10c})$$

$$F^{2me}(k_1, K_2, k_3, K_4) = -\frac{1}{\epsilon^2} \left[ (-s)^{-\epsilon} + (-t)^{-\epsilon} - (-K_2^2)^{-\epsilon} - (-K_4^2)^{-\epsilon} \right] \\ + \text{Li}_2\left(1 - \frac{K_2^2}{s}\right) + \text{Li}_2\left(1 - \frac{K_2^2}{t}\right) + \text{Li}_2\left(1 - \frac{K_4^2}{s}\right) + \text{Li}_2\left(1 - \frac{K_4^2}{t}\right) \\ - \text{Li}_2\left(1 - \frac{K_2^2 K_4^2}{st}\right) + \frac{1}{2} \ln^2\left(\frac{s}{t}\right), \quad (\text{IV.10d})$$

$$F^{1m}(k_1, k_2, k_3, K_4) = -\frac{1}{\epsilon^2} \left[ (-s)^{-\epsilon} + (-t)^{-\epsilon} - (-K_4^2)^{-\epsilon} \right] \\ + \text{Li}_2\left(1 - \frac{K_4^2}{s}\right) + \text{Li}_2\left(1 - \frac{K_4^2}{t}\right) + \frac{1}{2} \ln^2\left(\frac{s}{t}\right) + \frac{\pi^2}{6}, \quad (\text{IV.10e})$$

$$F^{0m}(k_1, k_2, k_3, k_4) = -\frac{1}{\epsilon^2} \left[ (-s)^{-\epsilon} + (-t)^{-\epsilon} \right] + \frac{1}{2} \ln^2\left(\frac{s}{t}\right) + \frac{\pi^2}{2}, \quad (\text{IV.10f})$$

where the  $k_i$  denote on-shell momenta and the  $K_i$  off-shell momenta. The kinematic variables are

$$s = (k_1 + k_2)^2, \quad t = (k_2 + k_3)^2, \quad (\text{IV.11})$$

or with  $k$  relabeled as  $K$  for off-shell (massive) legs and the functions appearing in  $F_4^{4m}$  are

$$\rho \equiv \sqrt{1 - 2\lambda_1 - 2\lambda_2 + \lambda_1^2 - 2\lambda_1\lambda_2 + \lambda_2^2}, \quad (\text{IV.12})$$

and

$$\lambda_1 = \frac{K_1^2 K_3^2}{(K_1 + K_2)^2 (K_2 + K_3)^2}, \quad \lambda_2 = \frac{K_2^2 K_4^2}{(K_1 + K_2)^2 (K_2 + K_3)^2}. \quad (\text{IV.13})$$

When dealing with the kinematics of an  $n$ -point amplitude it is convenient to label the integral functions in terms of the kinematic variables which may appear. Thus, we define

$$F_{n:r,r',r'';i}^{4m} = F^{4m}(k_i + \cdots + k_{i+r-1}, k_{i+r} + \cdots + k_{i+r+r'-1}, k_{i+r+r'} + \cdots + k_{i+r+r'+r''-1}, k_{i+r+r'+r''} + \cdots + k_{i-1}), \quad (\text{IV.14a})$$

$$F_{n:r,r';i}^{3m} = F^{3m}(k_{i-1}, k_i + \cdots + k_{i+r-1}, k_{i+r} + \cdots + k_{i+r+r'-1}, k_{i+r+r'} + \cdots + k_{i-2}), \quad (\text{IV.14b})$$

$$F_{n:r;i}^{2mh} = F^{2mh}(k_{i-2}, k_{i-1}, k_i + \cdots + k_{i+r-1}, k_{i+r} + \cdots + k_{i-3}), \quad (\text{IV.14c})$$

$$F_{n:r;i}^{2me} = F^{2me}(k_{i-1}, k_i + \cdots + k_{i+r-1}, k_{i+r}, k_{i+r+1} + \cdots + k_{i-2}), \quad (\text{IV.14d})$$

$$F_{n:i}^{1m} = F^{1m}(k_{i-3}, k_{i-2}, k_{i-1}, k_i + k_{i+1} + \cdots + k_{i-4}), \quad (\text{IV.14e})$$

$$F_4^{0m} \equiv F^{0m}(k_1, k_2, k_3, k_4), \quad (\text{IV.14f})$$

corresponding to the kinematics depicted in fig. 15. The labels on the momenta are defined mod  $n$ .

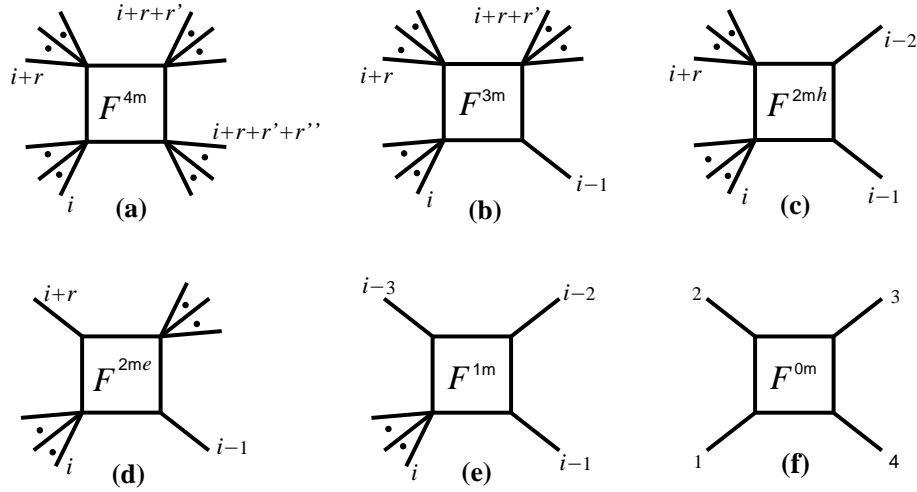


Figure 15. The kinematics of the box functions defined in eq. (IV.14).

For the purposes of this paper it is useful to exhibit the poles in eq. (IV.8) contained in the integral functions with  $n$ -point kinematics,

$$I_{4:r,r',r'';i}^{4m} = -2r \Gamma \frac{F_{n:r,r',r'';i}^{4m}}{t_i^{[r+r']} t_{i+r}^{[r'+r'']} \rho}, \quad (\text{IV.15a})$$

$$I_{4:r,r';i}^{3m} = -2r \Gamma \frac{F_{n:r,r';i}^{3m}}{t_{i-1}^{[r+1]} t_i^{[r+r']} - t_i^{[r]} t_{i+r+r'}^{[n-r-r'-1]}}, \quad (\text{IV.15b})$$

$$I_{4:r;i}^{2mh} = -2r \Gamma \frac{F_{n:r;i}^{2mh}}{t_{i-2}^{[2]} t_{i-1}^{[r+1]}}, \quad (\text{IV.15c})$$

$$I_{4:r;i}^{2me} = -2r \Gamma \frac{F_{n:r;i}^{2me}}{t_{i-1}^{[r+1]} t_i^{[r+1]} - t_i^{[r]} t_{i+r+1}^{[n-r-2]}}, \quad (\text{IV.15d})$$

$$I_{4:i}^{1m} = -2r \Gamma \frac{F_{n:i}^{1m}}{t_{i-3}^{[2]} t_{i-2}^{[2]}}, \quad (\text{IV.15e})$$



where the dimensionful prefactors have been extracted.

#### IV.4 Higher dimension scalar integrals

Due to the modified integral reduction procedure discussed in appendix I, higher-dimensional bubble, triangle and box functions may also appear in the basis of functions in terms of which amplitudes are expressed. These integrals may be obtained from the  $D = 4 - 2\epsilon$  integrals using the recursion formulas

$$I_n^{D=6-2\epsilon} = \frac{1}{(n-5+2\epsilon)c_0} \left( 2I_n - \sum_{i=1}^n c_i I_{n-1}^{(i)} \right), \quad (\text{IV.16})$$

$$I_n^{D=8-2\epsilon} = \frac{1}{(n-7+2\epsilon)c_0} \left( 2I_n^{D=6-2\epsilon} - \sum_{i=1}^n c_i I_{n-1}^{(i),D=6-2\epsilon} \right), \quad (\text{IV.17})$$

where

$$c_i = \sum_{j=1}^n S_{ij}^{-1}, \quad c_0 = \sum_{i=1}^n c_i = \sum_{i,j=1}^n S_{ij}^{-1}, \quad (\text{IV.18})$$

and

$$S_{ij} = -\frac{1}{2}(p_{i-1} - p_{j-1})^2, \quad (\text{IV.19})$$

is a symmetric matrix. As defined previously the  $(n-1)$ -point integral  $I_{n-1}^{(i)}$  is obtained by removing the internal propagator between external lines  $(i-1)$  and  $i$  from the original  $n$ -point (scalar) integral. The  $D = 6 - 2\epsilon$  bubble function is of particular interest and is

$$I_2^{D=6-2\epsilon}(K^2) = -\frac{r_\Gamma}{2\epsilon(1-2\epsilon)(3-2\epsilon)} (-K^2)^{1-\epsilon}. \quad (\text{IV.20})$$

For one- and two-external mass triangles eq. (IV.16) is ill-defined because the  $S_{ij}$  matrix is not invertible; in this case the  $D = 6 - 2\epsilon$  integrals may be obtained by direct integration [23] yielding

$$I_3^{1\text{m},D=6-2\epsilon}(K_1^2) = \frac{r_\Gamma}{2\epsilon(1-\epsilon)(1-2\epsilon)} (-K_1^2)^{-\epsilon}, \quad (\text{IV.21a})$$

$$I_3^{2\text{m},D=6-2\epsilon}(K_1^2, K_2^2) = \frac{r_\Gamma}{2\epsilon(1-\epsilon)(1-2\epsilon)} \frac{(-K_1^2)^{1-\epsilon} - (-K_2^2)^{1-\epsilon}}{K_2^2 - K_1^2}. \quad (\text{IV.21b})$$

Observe that all higher dimension scalar integrals are related to  $D = 4 - 2\epsilon$  dimensional scalar integrals by coefficients which depend on  $\epsilon$ . For the integrals which may be obtained from the recursion formulas (IV.16) and (IV.17), the  $\epsilon$ -dependence appears in the overall factor. Note also that the six-dimension triangles (IV.21) may be expressed in terms of the four-dimensional bubble function (IV.2) with rational coefficients containing explicit  $\epsilon$ -dependence.

As discussed in appendix I all  $\epsilon$ -dependence in integral reduction coefficients may be eliminated by including the  $D = 6 - 2\epsilon$  triangle functions and  $D = 8 - 2\epsilon$  box functions in the basis of integral functions in which amplitudes are expressed; the  $\epsilon$ -dependence is absorbed into the enlarged set of integral functions. Observe that the  $D = 6 - 2\epsilon$  scalar box is both infrared and ultraviolet finite we may drop the  $\epsilon$  in the overall coefficient in eq. (IV.16) with no effect through  $\mathcal{O}(\epsilon^0)$ ; thus  $I_4^{D=6-2\epsilon}$  may be written in terms of  $D = 4 - 2\epsilon$  integrals with no  $\epsilon$  appearing in the coefficients. There is thus no need to include  $I_4^{D=6-2\epsilon}$  in the basis of integral functions.

## References

- [1] Z. Bern, L. Dixon and D.A. Kosower, Phys. Rev. Lett. 70:2677 (1993).
- [2] Z. Kunszt, A. Signer and Z. Trócsányi, Phys. Lett. B336:529 (1994), hep-ph/9405386.
- [3] Z. Bern, L. Dixon and D.A. Kosower, Nucl. Phys. B437:259 (1995), hep-ph/9409393.
- [4] F.A. Berends, R. Kleiss, P. De Causmaecker, R. Gastmans and T. T. Wu, Phys. Lett. 103B:124 (1981);  
P. De Causmaecker, R. Gastmans, W. Troost and T.T. Wu, Nucl. Phys. B206:53 (1982);  
R. Kleiss and W.J. Stirling, Nucl. Phys. B262:235 (1985);  
J.F. Gunion and Z. Kunszt, Phys. Lett. 161B:333 (1985);  
Z. Xu, D.-H. Zhang and L. Chang, Nucl. Phys. B291:392 (1987).
- [5] Z. Bern and D.A. Kosower Nucl. Phys. B379:451 (1992).
- [6] Z. Bern and D.A. Kosower, Phys. Rev. Lett. 66:1669 (1991);  
Z. Bern, Phys. Lett. 296B:85 (1992);  
K. Roland, Phys. Lett. 289B:148 (1992);  
M.J. Strassler, Nucl. Phys. B385:145 (1992);  
C.S. Lam, Nucl. Phys. B397:143 (1993); Phys. Rev. D48:873 (1993);  
Z. Bern, D.C. Dunbar and T. Shimada, Phys. Lett. 312B:277 (1993), hep-th/9307001;  
G. Cristofano, R. Marotta and K. Roland, Nucl. Phys. B392:345 (1993);  
M.G. Schmidt and C. Schubert, Phys. Lett. 318B:438 (1993); Phys. Lett. B331:69 (1994);  
D. Fliegner, M.G. Schmidt and C. Schubert, Z. Phys. C64:111 (1994), hep-ph/9401221;  
D.C. Dunbar and P.S. Norridge, Nucl. Phys. B433:181 (1995), hep-th/9408014;  
P. Di Vecchia, A. Lerda, L. Magnea and R. Marotta, preprint hep-th/9502156.
- [7] M.T. Grisaru, H.N. Pendleton and P. van Nieuwenhuizen, Phys. Rev. D15:996 (1977);  
M.T. Grisaru and H.N. Pendleton, Nucl. Phys. B124:81 (1977);  
S.J. Parke and T. Taylor, Phys. Lett. 157B:81 (1985);  
Z. Kunszt, Nucl. Phys. B271:333 (1986).
- [8] F.A. Berends and W.T. Giele, Nucl. Phys. B306:759 (1988);  
D.A. Kosower, Nucl. Phys. B335:23 (1990).
- [9] G.D. Mahlon, Phys. Rev. D49:2197 (1994); Phys. Rev. D49:4438 (1994).
- [10] Z. Bern, L. Dixon, D.C. Dunbar and D.A. Kosower, Nucl. Phys. B425:217 (1994), hep-ph/9403226.
- [11] Z. Bern, L. Dixon, D.C. Dunbar and D.A. Kosower, Nucl. Phys. B435:59 (1995), hep-ph/9409265.
- [12] F.A. Berends and W.T. Giele, Nucl. Phys. B313:595 (1989).
- [13] Z. Bern, G. Chalmers, L. Dixon and D.A. Kosower, Phys. Rev. Lett. 72:2134 (1994), hep-ph/9312333.
- [14] Z. Bern, L. Dixon and D.A. Kosower, hep-th/9311026, in *Proceedings of Strings 1993*, eds. M.B. Halpern, A. Sevrin and G. Rivlis (World Scientific, 1994), hep-th/9311026.
- [15] G. Chalmers, hep-ph/9405393, in *Proceedings of the XXII ITEP International Winter School of Physics* (Gordon and Breach, 1995).
- [16] Z. Kunszt, A. Signer and Z. Trócsányi, Nucl. Phys. B411:397 (1994).
- [17] G. Altarelli and G. Parisi, Nucl. Phys. B126:298, (1977);  
G. Curci, W. Furmanski and R. Petronzio, Nucl. Phys. B175:27 (1980).
- [18] G. Chalmers, (unpublished).

- [19] Z. Kunszt and D. Soper, Phys. Rev. D46:192 (1992).
- [20] W.T. Giele and E.W.N. Glover, Phys. Rev. D46:1980 (1992);  
W.T. Giele, E.W.N. Glover and D. A. Kosower, Nucl. Phys. B403:633 (1993).
- [21] Z. Kunszt, A. Signer and Z. Trócsányi, Nucl. Phys. B420:550 (1994).
- [22] A. Denner, U. Nierste and R. Scharf, Nucl. Phys. B367:637 (1991);  
N.I. Usyukina and A.I. Davydychev, Phys. Lett. 298B:363 (1993); Phys. Lett. 305B:136 (1993).
- [23] Z. Bern, L. Dixon and D.A. Kosower, Nucl. Phys. B412:751 (1994), hep-ph/9306240.
- [24] J.E. Paton and Chan Hong-Mo, Nucl. Phys. B10:519 (1969);  
F.A. Berends and W.T. Giele, Nucl. Phys. B294:700 (1987);  
M. Mangano, S. Parke and Z. Xu, Nucl. Phys. B298:653 (1988);  
M. Mangano, Nucl. Phys. B309:461 (1988).
- [25] M. Mangano and S.J. Parke, Phys. Rep. 200:301 (1991).
- [26] Z. Bern and D.A. Kosower, Nucl. Phys. B362:389 (1991).
- [27] S.J. Parke and T.R. Taylor, Phys. Rev. Lett. 56:2459 (1986).
- [28] W. Siegel, Phys. Lett. 84B:193 (1979);  
D.M. Capper, D.R.T. Jones and P. van Nieuwenhuizen, Nucl. Phys. B167:479 (1980).
- [29] J.C. Collins, *Renormalization* (Cambridge University Press, 1984).
- [30] G. 't Hooft and M. Veltman, Nucl. Phys. B44:189 (1972).
- [31] T. Muta, *Foundations of Quantum Chromodynamics: an introduction to perturbative methods in gauge theories*, (World Scientific, 1987).
- [32] Z. Bern and D.C. Dunbar, Nucl. Phys. B379:562 (1992).
- [33] L.F. Abbott, Nucl. Phys. B185:189 (1981);  
L.F. Abbott, M.T. Grisaru and R.K. Schaefer, Nucl. Phys. B229:372 (1983).
- [34] J.L. Gervais and A. Neveu, Nucl. Phys. B46:381 (1972).
- [35] M.B. Green, J.H. Schwarz and L. Brink, Nucl. Phys. B198:474 (1982).
- [36] L.M. Brown and R.P. Feynman, Phys. Rev. 85:231 (1952);  
L.M. Brown, Nuovo Cimento 21:3878 (1961);  
G. 't Hooft and M. Veltman, Nucl. Phys. B153:365 (1979);  
R.G. Stuart, Comp. Phys. Comm. 48:367 (1988);  
R.G. Stuart and A. Gongora, Comp. Phys. Comm. 56:337 (1990).
- [37] G. Passarino and M. Veltman, Nucl. Phys. B160:151 (1979).
- [38] B. Petersson, J. Math. Phys., 6:1955 (1965);  
G. Kallen and J.S. Toll, J. Math. Phys., 6:299 (1965);  
D.B. Melrose, Il Nuovo Cimento 40A:181 (1965).
- [39] W. van Neerven and J.A.M. Vermaseren, Phys. Lett. 137B:241 (1984);  
G.J. van Oldenborgh and J.A.M. Vermaseren, Z. Phys. C46:425 (1990).
- [40] Z. Bern, L. Dixon and D.A. Kosower, Phys. Lett. 302B:299 (1993); erratum *ibid.* 318B:649 (1993).
- [41] L. Lewin, *Dilogarithms and Associated Functions* (Macdonald, 1958).
- [42] Z. Bern, hep-ph/9304249, in *Proceedings of Theoretical Advanced Study Institute in High Energy Physics (TASI 92)*, eds. J. Harvey and J. Polchinski (World Scientific, 1993);  
Z. Bern and A. Morgan, Phys. Rev. D49:6155 (1994), hep-ph/9312218.